Study of thermodynamic properties of $U\_1-yPu\_yO\_2$ MOX fuel using classical molecular Monte Carlo simulations

Cyrille Takoukam Takoundjou, Emeric Bourasseau, Véronique Lachet

Study of thermodynamic properties of $U_{1-y}Pu_yO_2$ MOX fuel using classical molecular Monte Carlo simulations

Cyrille Takoukam Takoundjou[1], Emeric Bourasseau[1], Véronique Lachet[2]

[1]CEA, DEN, DEC, F - 13108 Saint Paul-lez-Durance, France
[2]IFP Energies nouvelles, 1 et 4 avenue de Bois-Préau, 92852 Rueil-Malmaison, France

Abstract

The molecular Monte Carlo method, combined with the CRG interatomic potential, is used for the first time to investigate stoichiometric mixed oxides $U_{1-y}Pu_yO_2$ (with y in the range 0 to 1). The implementation of this Monte Carlo method for mixed oxides simulation was carried out involving two algorithms, with and without cation exchange. The use of these two Monte Carlo algorithms allowed us to test the effect of the substitutional disorder implied by the coexistence of two types of cations. Structural, thermodynamic, and mechanical properties of the stoichiometric mixed oxides fuel $U_{1-y}Pu_yO_2$ have been investigated over a wide temperature range (from 300 K to the melting temperature) and plutonium content (from 0 to 100 atom %). Our study shows that the exploration of cationic configurations through the cation exchange algorithm is required for a complete description of the mixed oxides fuel properties, especially for the atomic structural properties. Concerning thermodynamic properties, the evolution of the computed specific heat as a function of temperature exhibits one peak for all plutonium contents around 2300 K, *i.e.* at ~0.8 T_m (T_m is the melting temperature). The same behaviour is observed for the linear thermal expansion coefficient. These peaks, also observed in previous studies, are related to the Bredig transition known to occur around 0.8 T_m. A good agreement between our results, experiments, and previous calculations is found for temperatures up to about 2100 K. Above this temperature, our calculations show a behaviour different from experimental recommendations.

1. Introduction

Uranium dioxide UO_2 has been widely studied as the conventional fuel for Light Water Reactors (LWR). It can also be blended with other actinide powders, such as PuO_2, to form Mixed Oxide (MOX) fuels. To date, MOX fuel is used in Light Water Reactors with a low Pu content (~9 at %). Fuel recycling helps save resources, reduces waste and amount of spent nuclear fuel from LWR, and burn minor actinides. In order to encourage fuel recycling, MOX fuel is envisaged as the reference fuel for generation IV Sodium Fast neutron Reactors (SFR) with a higher Pu content (between 25-30 at %). To ensure safety and fuel performance in the fuel qualification process, a complete investigation of MOX properties is required. Extensive knowledge of structural, mechanical and thermodynamic properties, among others is essential for fuel performance codes. However, experimental studies of Pu and its compounds are challenging to handle due to the high toxicity of plutonium. Therefore, atomistic simulation could be an alternative way of obtaining these properties.

In the literature, UO_2 has been widely investigated compared to PuO_2 and MOX fuels for which experimental thermodynamic data (thermal expansion, enthalpy, heat capacity…) are poorly known, especially at high temperatures (over 2000 K). Usually, experimental thermodynamic data are used to develop empirical correlations (so-called recommendations) used to describe the properties of the materials. However, due to a lack of experimental data on PuO_2 and MOX fuel, it is impractical to establish recommendations for these compounds. Kopp Neumann additivity law is often used as an alternative for the determination of MOX thermodynamic properties from UO_2 and PuO_2 recommendations. Moreover, several authors in the literature [1], [2] consider the recommendations of MOX to be the same as those for UO_2. Nonetheless, these recommendations are not based on updated data (such as the melting temperature, enthalpy, and heat capacity). Therefore, recommendations fail to reproduce correctly some material behaviours, such as the Bredig transition, which is known to occur at 0.8 Tm (melting temperature) [3], [4]. Such transition can be observed in several ionic materials, which can exhibit properties more reminiscent of simple liquids than of ideal crystalline materials when subject to an increase of the temperature or pressure. Around the critical temperature or pressure at which such transition appears, the atomic diffusion in these materials approaches the values usually observed in fluids at high temperatures. These materials discovered about 200 years ago by Faraday [5], [6] are called "superionic" as they can conserve their ionic composition at critical temperature. Superionic materials are usually classified as follows:

(i) type I superionic materials, which exhibit a first-order solid-solid structural transition, which has a noticeable effect on direct materials properties such as lattice parameter of anion sublattice and pair distribution functions.

(ii) type II superionic materials, which show a kink in their derivative properties (such as heat capacity at constant pressure and thermal expansion coefficient) at a critical temperature (T_λ). At T_λ, the heat capacity at constant pressure and the thermal expansion coefficient exhibit peaks, that are the signature of a second-order or some higher order "rounded" thermodynamic transition [7]. In actinide oxides, this transition is also termed "Bredig transition" or "lambda transition" [3], [8].

To date, all the theoretical studies carried out on MOX using empirical potentials are restricted to the use of Molecular Dynamic (MD) simulations. Several properties of MOX have been investigated using different potential forms. Yamada *et al*. [9] published one of the first studies on MOX using a Born-Mayer-Huggins interatomic potential [10], [11], and dealing with the thermophysical properties of PuO_2 and MOX fuel. In this work, a Morse potential term [9], [12] has been added to account for the covalent bonding between anions and cations. The authors evaluated the lattice parameter, heat capacity, compressibility, oxygen diffusivity and thermal conductivity of PuO_2 and MOX with 0.2 % of Pu. This study was extended by Kurosaki *et al*. [13] to higher temperatures (up to 3000 K). Arima *et al*. [10], [14] expand from the previous study by using only a Born-Mayer-Huggins interatomic potential for more extensive ranges of Pu content. However, these studies failed to reproduce bulk modulus and thermal conductivity at high temperatures (over 2000 K). Furthermore, the results obtained differed from one author to another depending on the empirical potential used [14]–[16]. These differences indicate the strong dependence of the results to the chosen potential form as well as the data (lattice parameter, thermal expansion and elastic constants at room temperature) on which the potential parameters were fitted. Recently, Cooper *et al*. [17] proposed a more sophisticated form of potential adding a many-body term to the pair-type contributions, through the Embedded Atom Model (EAM), to account for the many-body interactions in the compounds. The results obtained with the CRG potential reproduce correctly many measured properties of many actinide oxides and their mixed oxides for temperatures up to the melting temperature.

Molecular Dynamic (MD) consists in determining the trajectory of atoms by solving Newton's equations of motion of the system. During MD simulations of solids, atoms move slightly around their equilibrium positions, but the simulation time (limited to a few tens of nanoseconds) is not necessarily long enough to observe the atoms moving from one crystalline site to another. This constitutes a limitation of MD for the simulation of mixed oxide $U_{1-y}Pu_yO_2$. Stoichiometric $U_{1-y}Pu_yO_2$ mixed oxide is known to form an ideal solid solution [18], [19] (i.e. cations are randomly distributed in the face cubic centered sublattice). Exploring the cation distribution repartition during the simulation requires allowing the system to reach its real thermodynamic equilibrium state. Therefore, the use of MD to simulate mixed oxides might not be a relevant approach, since the initial cation repartition will be kept fixed during the simulation. Alternatively, the molecular Monte Carlo (MC) [20] simulation approach is expected to be more relevant since it can enable the exchange of uranium and plutonium atoms during a simulation, which allows for exploring the space of the cationic configurations to achieve the real thermodynamic equilibrium. The latter method has been successfully applied by Allan *et al*. [21] and Lavrentiev *et al*. [22] for the determination of the phase diagram and the thermodynamic properties of CaO/MgO system. In addition, the MC method has also been used in the literature to predict adsorption in porous materials such as MOFs, ZIFs, and Zeolites [23], [24].

In this study, molecular Monte Carlo simulations are performed for the first time to investigate the structural, mechanical, and thermodynamic properties of $U_{1-y}Pu_yO_2$, from 300 K to the melting temperature and from 0 to 100 % of Pu. This corresponds to a large amount of calculations, and as a consequence, we have used a classical potential to calculate atomic interactions as it is less computationally demanding than electronics calculations. The CRG empirical potential function from Cooper *et al.* [17] was chosen for this study since it was thoroughly tested by several authors [15], [25], [26]. The present article is organized as follows: in section 2, we describe the simulation conditions and the CRG empirical potential. Section 3 is dedicated to a study of the effects of cation exchanges, followed in section 4, by the presentation of the thermodynamic properties obtained using the molecular simulations. Results concerning the lattice parameter, thermal expansion, the linear thermal expansion coefficient, compressibility coefficient, bulk modulus, the enthalpy, and heat capacity are presented and discussed. The results are systematically compared to experimental data available and the recommendations. Finally, conclusions and perspectives are given in section 5.

2. Methods

MC simulations are carried out within the isobaric-isothermal (NPT) ensemble: both the atomic coordinates and the cell dimensions are allowed to vary during the simulations. We systematically compared two types of calculations: one without exchange of uranium and plutonium atoms, and one with cation exchanges. In the two cases, the temperature effect is take into account by allowing random translations of randomly selected atoms, and the pressure effect is obtained using random volume changes of the simulation box. In the first case, the attempt probabilities attributed to these MC moves are 99 % and 1 % respectively. This first case is fully comparable to MD simulations in the NPT ensemble. In the second case, a third move is also used to account for the effect of the cationic repartition: an exchange move between randomly selected uranium and plutonium atoms [27]. In this second case, the attempt probabilities attributed to these 3 MC moves are 79 %, 1 %, and 20 % respectively. In all calculations, each move attempt is accepted or rejected following a standard Metropolis scheme based on the potential energy difference between the old and new configurations [20]. The maximum variations in the atomic displacements and the volume changes are adjusted automatically during the simulation to maintain an acceptance/rejection ratio of approximately 0.4.

The values of thermodynamic properties are averaged on 500 million configurations. Simulations are performed with the MC GIBBS code [28], [29].

The empirical potential used to describe interactions between atoms in this work is the CRG potential [17], which combines a pair potential description with the many-body Embedded Atom Model (EAM) [30] from Daw and Baskes. In the CRG empirical potential, the potential energy E_i between an atom i with respect to all other atoms is given by:

$$\boldsymbol{E_i = \frac{1}{2}\sum_j U_{\alpha\beta}(r_{ij}) - G_\alpha\left(\sum_j \sigma_\beta(r_{ij})\right)^{\frac{1}{2}}} \qquad \text{Eq. 2.1}$$

This equation has two distinct components. $U_{\alpha\beta}(r_{ij})$ represents the pairwise interaction between two atoms i and j separated by distance r_{ij}. α and β are used to label the species of atom i and j respectively. The pairwise interaction terms are described using both long-range (Coulomb, $U_C(r_{ij})$) and short-range (Buckingham, $U_B(r_{ij})$ and Morse, $U_M(r_{ij})$) contributions as given by the equations (Eq. 2.2 to Eq. 2.5) below.

$$\boldsymbol{U_{\alpha\beta}(r_{ij}) = U_C(r_{ij}) + U_B(r_{ij}) + U_M(r_{ij})} \qquad \text{Eq. 2.2}$$

$$\boldsymbol{U_C(r_{ij}) = \frac{q_\alpha q_\beta}{4\pi\varepsilon_0 r_{ij}}} \qquad \text{Eq. 2.3}$$

$$\boldsymbol{U_B(r_{ij}) = A_{\alpha\beta} exp\left(-\frac{r_{ij}}{\rho_{\alpha\beta}}\right) - \frac{C_{\alpha\beta}}{r_{ij}^6}} \qquad \text{Eq. 2.4}$$

$$\boldsymbol{U_M(r_{ij}) = D_{\alpha\beta}\begin{bmatrix} exp\left(-2\gamma_{\alpha\beta}\left(r_{ij} - r_{\alpha\beta}^0\right)\right) \\ -2exp\left(-\gamma_{\alpha\beta}\left(r_{ij} - r_{\alpha\beta}^0\right)\right)\end{bmatrix}} \qquad \text{Eq. 2.5}$$

The parameters q_α, q_β, $A_{\alpha\beta}$, $\boldsymbol{\rho_{\alpha\beta}}$, $C_{\alpha\beta}$, $D_{\alpha\beta}$, $\gamma_{\alpha\beta}$ and $r_{\alpha\beta}^0$ are the parameters of these equations given in Table 1.

The second component of equation Eq. 2.1 represents the many-body EAM interaction term added by Cooper *et al.* to improve the pair interaction model. The pair interatomic potentials fail to reproduce the Cauchy's violation observed in actinide oxides with fluorite type structure (i.e. $C_{12} \neq C_{44}$ where C_{ij} are elastic tensor elements in Voigt notation). σ_β in this equation is computed as shown in equation Eq.2.6. In this equation, a short-range cut-off as an error function is applied at 1.5 Å that reduces the EAM component gradually to prevent unrealistic forces occurring at short separations; ensuring that there is no discontinuity in the interatomic energy, which would arise from an abrupt cut-off as pointed by Cooper *et al*. [31]. The function erf [31] stands for the error function and the parameters η_β and G_α are presented in Table 2.

$$\boldsymbol{\sigma_\beta(r_{ij}) = \frac{1}{2}\left(\frac{\eta_\beta}{r_{ij}^8}\right)\{1 + erf[20(r - 1.5)]\}} \qquad \text{Eq. 2.6}$$

Table 1. Parameters of the interatomic CRG empirical potential [17]. M stands for U and Pu cations. The parameter in bold is the refitted one, which predicts the correct melting PuO_2 temperature at 2800 ± 50 K, as proposed by Cooper *et al*., in a second article [31].

q(|e|)	M	2.2208
	O	-1.1104
A(eV)	M-M	18600
	U-O	448.779
	Pu-O	**527.516**
	O-O	830.283
ρ(Å)	U-U	0.2747
	Pu-Pu	0.2637
	U-O	0.3878
	Pu-O	0.3793
	O-O	0.3529
C(eV.Å^6)	M-M	0.00
	M-O	0.00
	O-O	3.8843
D(eV)	U-O	0.6608
	Pu-O	0.7019
ɣ(Å^{-1})	U-O	2.058
	Pu-O	1.980
r^0(Å)	U-O	2.381
	Pu-O	2.346

Table 2. Parameters of the many-body EAM term used within the CRG empirical potential [17]. The parameters in bold are the refitted one which predicts the melting PuO_2 temperature at 2800 ± 50 K as proposed by Cooper *et al.,* in a second article [31].

	$G_\alpha[eV.Å^{1.5}]$	$\eta_\beta[Å^5]$
U	1.806	3450.995
Pu	**2.168**	**3980.058**
O	0.69	106.856

A 2592 atom (864 cations and 1728 anions) supercell is used. It corresponds to a 6×6×6 time replication of a 12 atom cubic supercell of the MO_2 fluorite structure. Several methods are used in the literature to model the chemical disorder of two different atoms in size limited systems of binary alloys [32]–[36]: in particular the Virtual-Crystal Approximation (VCA) method [35], the Site-Coherent-Potential-Approximation (SCPA) [33] method and the Special Quasi-random Structure (SQS) [32] method. The first two approaches are "structureless" since they do not account for the local structure relaxations, which impact local properties averaging. They only consider the average occupations by <A> , <B>, or <AB> of sites in the case of A-B alloys, removing the information associated with the geometrical arrangements of atoms around the sites. In the VCA method, the alloy is assumed to have a single <AB> averaged type of atom while the SCPA method assumes all A and separately all B are equivalent (composed of chemical species having similar size), and each is

embedded in a uniform medium. The method commonly used for small size supercells of binary alloy is the SQS method developed by Zunger *et al*. [32]. Pezold *et al*. [37] have also used a Monte-Carlo-based search scheme to construct a set of SQS structures covering the entire concentration range. The SQS method allows building configurations of binary alloys accounting for the substitutional disorder based on the reproduction of the pair correlation functions at rather short distances. This approach becomes difficult to handle for the large supercells, especially larger than 96 atoms, whereas modeling an ideal solid solution requires a large supercell in order to represent the random distribution in the mixture correctly. For this reason, we built larger supercells containing 2592 atoms by duplicating the SQS 96 atom supercells (see Figure 1.a) in the three spatial directions. These supercells represented our initial configurations (see Figure 1.b). All the initial configuration used in this work (for calculations with or without cation exchanges) are built in this way and contained 2592 atoms. The arrangements of U and Pu cations from Pezold *et al*., [37] are used for the whole range of Pu content.

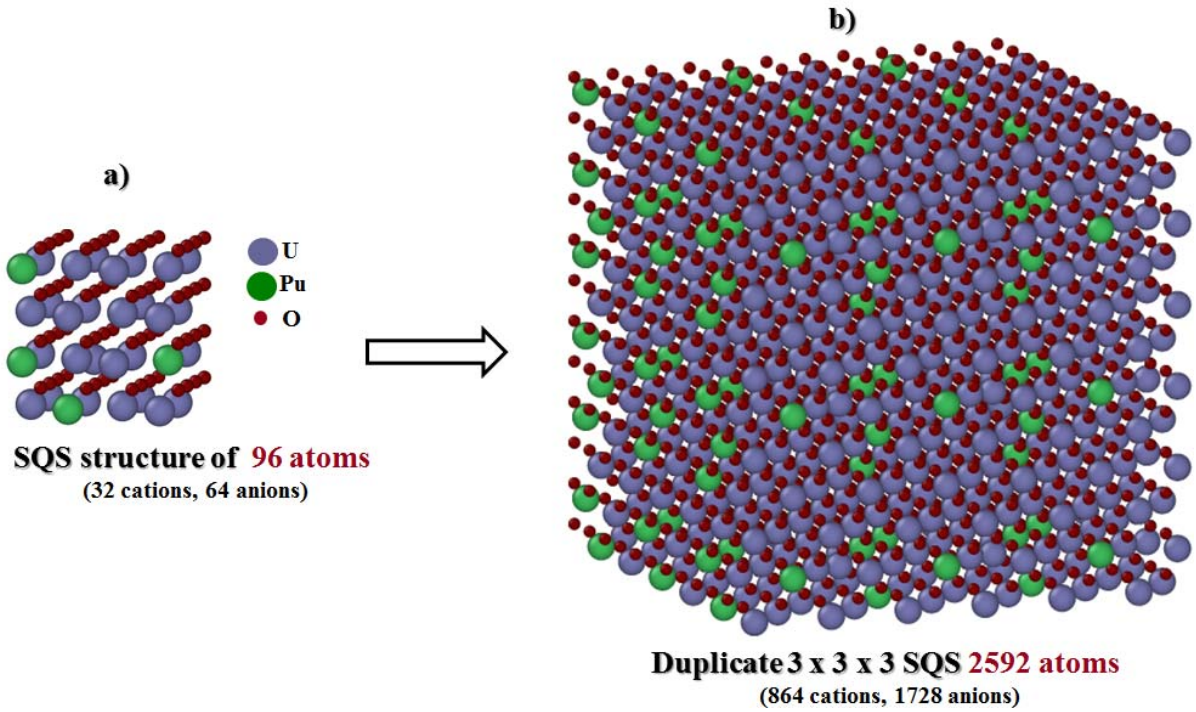

Figure 1: SQS 96 atom supercells with 25% Pu content a) and 3 x 3 x 3 SQS duplication in the three spatial directions to obtain 2592 atoms. All the initial configurations used in this work are built in this way.

3. Effect of the MC cation exchange algorithm and deviation from the ideal solid solution

3.1. Effect on thermodynamic properties

In order to measure the effect of cation exchanges in our MC simulations, we have compared results from MC simulations with and without cation exchanges.

Table 3 shows the various calculated thermodynamic properties, namely lattice parameter (a), enthalpy (H), linear thermal expansion coefficient (α), bulk modulus (B) and heat capacity (C_p) of stoichiometric $U_{0.75}Pu_{0.25}O_2$ obtained at room temperature. In this work, the enthalpy is defined as $H = U + PV = 9/2 * RT + Uconf + PV$. Were U, P, and V are respectively the energy, the pressure

and the volume of the system. The energy U can also be written as the sum of the configurational energy of the system Uconf (the energy coming from the CRG potential) and a perfect gas (or kinetic) contribution equal to 9/2*RT (corresponding to the energy of an isolated UO_2 molecule). All the computed properties in Table 3 are obtained using both algorithms, with and without cation exchanges. Results are also compared with *ab initio* and experimental measurements available in the literature [38], [39], [40], [41]. Concerning α and C_p from MC in Table 3, they are both computed respectively by analyzing the volume fluctuations, following the equation Eq 4.2, and by analyzing the energy fluctuations, following the equation Eq 4.5. As shown in this table, the computed values of lattice parameter and enthalpy for both algorithms are identical. Moreover, these values are consistent with the experimental data as well as with *ab initio* MD results. Concerning derivative properties (linear thermal expansion, bulk modulus and heat capacity), the values given by the two algorithms show a slight difference, less than 0.3%, which is smaller than statistical uncertainty. Therefore, no effect of the cation exchange algorithm was detected with respect to the thermodynamic properties. Besides, our computed heat capacity at room temperature showed an overestimation by roughly 17% of experimental and *ab initio* values. This was discussed in more details in section 4. All the other calculated properties using both algorithms matched reasonably well with the experimental [39], [38], [40], [41] as well as *ab initio* results [42], [43]. To conclude, both algorithms are equivalent to compute the thermodynamic properties of MOX.

Table 3. Lattice parameter (a), enthalpy (H), linear thermal expansion coefficient (α), bulk modulus (B), and heat capacity (C_p) of $U_{0.75}Pu_{0.25}O_2$ solid solution computed at 300 K using MC simulation method with and without cation exchanges. These results are compared to *ab initio* and experimental data available in the literature. Concerning *ab initio* results, reported lattice parameter and bulk modulus are computed using static calculation (at 0 K) while the heat capacity is obtained using *ab initio* MD at 300 K.

	MC without cationic exchange	MC with cationic exchange	*Ab initio*	Experimental
a (Å)	$5.45 \pm (1.06\ 10^{-5})$	$5.45 \pm (1.06\ 10^{-5})$	5.52 (± 1.3 %) [a]	5.46 [c]
$H(10^6.J.mol^{-1})$	$-3.94 \pm (2.10\ 10^{-4})$	$-3.94 \pm (2.10\ 10^{-4})$	-	-
$\alpha\ (10^{-5}.K^{-1})$	2.95 ± 0.11	2.96 ± 0.11	-	2.93 [d]
B (GPa)	207 ± 3	207 ± 3	197 [a]	209[e]
$C_p\ (J.mol^{-1}.K^{-1})$	75.70 ± 0.27	75.62 ± 0.27	64.43 [b]	*64.63 [f]

[a]ref [42]. [b]ref [43]. [c]ref [38]. [d]ref [39]. [e]ref [40]. [f]ref [41]. *measurement is for 28% Pu content

3.2. Effect on structural properties: interatomic distances and oxygen tetrahedron distribution

We also checked the influence of the cation exchanges algorithm on structural properties such as pair distribution functions (PDF) and interatomic distances. It is well established in the literature that stoichiometric $U_{1-y}Pu_yO_2$ crystalizes in the fluorite-type structure [18], [44] in which U and Pu cations are distributed in the face-centered cubic lattice to form the cation sublattice. In this cation sublattice, the substitution of U cations by Pu cations (and vice versa) slightly modifies the interatomic distances between uranium or plutonium and oxygen atoms compared to pure oxides. As shown by Njifon *et al.* [42] using DFT calculations, the U-O interatomic distance decreases with the addition of plutonium atoms by comparison to its value in UO_2, which is in agreement with the XAS (X-ray Absorption Spectroscopy) experiments. For MC simulations (see Table 4), our calculated interatomic distances

are identical whatever the algorithm used. These distances are also identical to those obtained in pure oxides UO_2 and PuO_2. These results probably come from the empirical potential which was fitted only on the pure actinide oxide properties. However, the differences between our calculated distances, *ab initio* results and the experimental measurements are of the same order of magnitude as the uncertainty on the lattice parameter ($1.06* 10^{-5}$ Å).

Table 4. The interatomic distances M-O (with M=U or Pu) in $U_{0.70}Pu_{0.30}O_2$, UO_2, and PuO_2 within the first coordination shell in comparison with both experimental XAS [19] and *ab initio* theoretical work [42]. The *ab initio* values were obtained for $U_{0.75}Pu_{0.25}O_2$ solid solution. All interatomic distances are given in Å.

	MC without cationic exchange		MC with cationic exchange		*Ab initio* MD		Experimental	
	d_{U-O}	d_{Pu-O}	d_{U-O}	d_{Pu-O}	d_{U-O}	d_{Pu-O}	d_{U-O}	d_{Pu-O}
$U_{0.70}Pu_{0.30}O_2$	2.35	2.33	2.35	2.33	2.38	2.37	2.35	2.35
UO_2	2.35				2.40		2.37	
PuO_2		2.33						2.33

In the fluorite structure, the anions are located at the center of the tetrahedrons formed by 4 cations. In the MOX, each oxygen atom is then located at the center of a cationic tetrahedron formed by U and Pu cations with 5 possible configurations, since the number of Pu can vary from 0 to 4. The distribution of these 5 types of tetrahedrons in a sample varies with the plutonium content and the potential used to describe the local interactions between cations in the system. We considered a sample of stoichiometric MOX $(U,Pu)O_2$ with 30% Pu content. The investigation at room temperature of the distributions of the 5 types of tetrahedrons is carried out first without the cation exchange algorithm, and then with the cation exchange algorithm.

Figure 2 shows the average tetrahedron distribution calculated using both algorithms as a function of the number of plutonium around each oxygen atom in $U_{0.70}Pu_{0.30}O_2$. The results are compared to the experimental tetrahedron distribution obtained by Vigier *et al*. [19] using ^{17}O NMR (Nuclear Magnetic Resonance), as well as with the theoretical distribution corresponding to the stoichiometric $U_{0.70}Pu_{0.30}O_2$ ideal solid solution [19]. This figure shows that the curve obtained with cation exchanges is closer to the experimental curve than the one obtained without cation exchange, proving that MC simulations with cation exchanges yield a better description of the real distribution. Small differences are found when we comparing the experimental curve by Vigier *et al.,* with that of a random theoretical distribution representing an ideal solid solution. Despite these differences, Vigier *et al*. have concluded that their experimental sample was an ideal solid solution. Our results using cation exchanges is closer to random theoretical distribution of an ideal solid solution than to the experimental distribution. Therefore, we conclude that the MC method with the cation exchange algorithm associated with the CRG empirical potential reproduce well the random distribution of cations expected in the theoretical ideal solid solution. Experimentally, according to the authors, experimental distribution, no signal was detected for tetrahedrons containing 4 Pu. The concentration of the tetrahedrons containing 4 Pu was too low for a 30 % Pu content sample to be detected by ^{17}O NMR. The MC computed value for tetrahedron with 4 plutonium atoms was about 1%.

Since our results do not reproduce perfectly the experimental distribution, it is interesting to investigate other structural information such as the number of Pu in the first cationic coordination shell and the evolution of the U/M fraction.

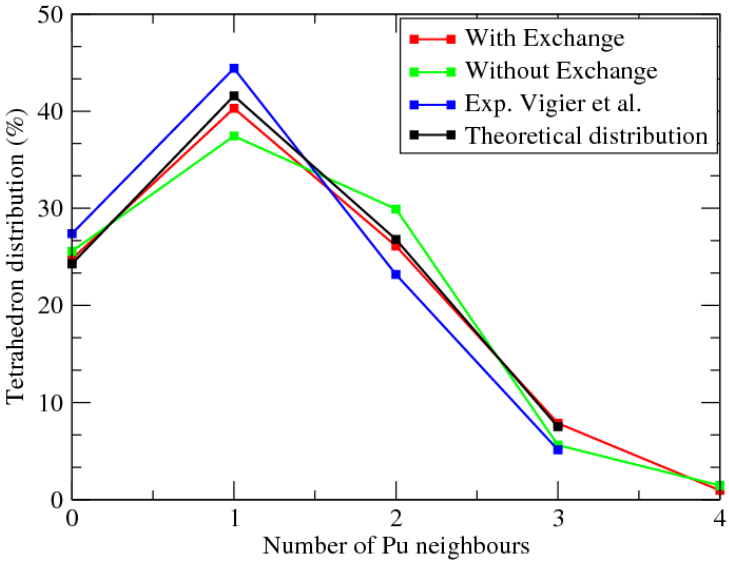

Figure 2: Tetrahedron distribution around an oxygen atom as a function of the number of Pu neighbours in $U_{0.70}Pu_{0.30}O_2$ at 300 K using MC simulation algorithms with and without cation exchanges. The results are presented along with the random theoretical distribution of an ideal solid solution and experimental distribution by Vigier *et al*. [19].

3.3. Effect on U/M fraction and on number of Pu atoms in the first coordination shell

To investigate with more detail the atomic structure, we first studied the pair distribution functions (PDF) between cations. The number of plutonium around a given plutonium cation is determined through the integration of the Pu-Pu PDF. These results are shown in Figure 3 as a function of interatomic distances for $U_{0.75}Pu_{0.25}O_2$ at 300 K and 1000 K with a focus on the first coordination shell around a Pu in the cation sublattice (between 4 and 5 Å). In the fluorite structure, twelve cations (U and Pu) can be found in the first cation coordination shell. In the case of a plutonium content of 25 %, three plutoniums are expected around a given plutonium cation. As shown in Figure 3, three neighbouring plutonium cation are found for the two temperatures studied when cation exchange is not allowed. This shows that during the MC simulation process without cation exchange, the cationic repartition remained frozen in the initial configuration coming from SQS despite the effect of temperature. In contrast, in MC simulations with cation exchange, the number of plutonium in the first coordination shell of a given plutonium reaches values higher than three. This observation demonstrated that during the MC simulation process using cation exchange algorithm the system did not remain frozen in the initial cationic configuration. The results also shows that the Pu atoms tend to cluster with each other, leading to a small deviation from the ideal solid solution. The slight clustering of Pu atoms is higher at 300 K than at 1000 K. However, this effect is tenuous and accounts for a difference of only 3.33 %.

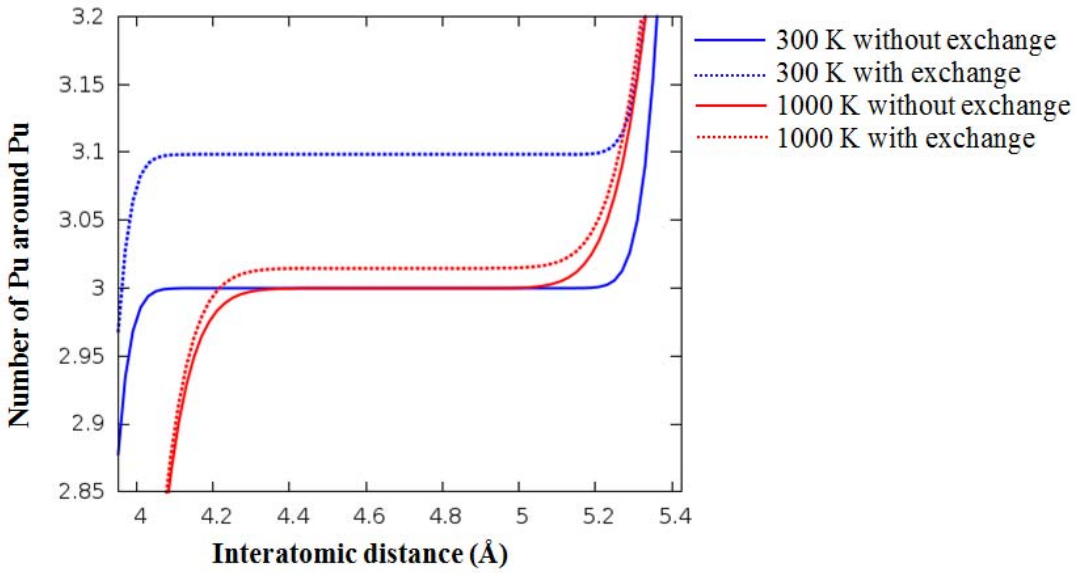

Figure 3: Variation of integrated Pu-Pu pair distribution function (PDF) in $U_{0.75}Pu_{0.25}O_2$ at 300 K and 1000 K as a function of interatomic distance. The solid lines stand for the simulations without cation exchanges and the dashed lines for the simulations with cation exchanges.

The phenomena shown in Figure 3 can be confirmed by analyzing the U/M fraction with M being U+Pu. This U/M fraction is the ratio between the number of U atoms and the total number of U and Pu cations in the system. It is obtained by combining the integrated U-U and U-Pu pair distribution functions. Figure 4 shows the U/M fraction as a function of pair distance for the MOX containing 25 % of plutonium. Given 25 % of plutonium, the U/M fraction is expected to be 0.75 in our system. For the algorithm without exchanges, a 0.75 ratio is obtained at short distances for both investigated temperatures, while significant lower values are obtained at long distances. For cation exchange, the U/M fraction is slightly higher than 0.75 at short distances and is exactly equal to 0.75 at long distances, implying that the U atoms tended to cluster at short distances. Moreover, the fact that the U/M fraction decreases considerably at long distance for all temperatures studied without cation exchange is a proof that the duplication of SQS supercells does not lead to a good description of a random distribution of cations beyond the second shell.

To conclude on this part, the MC simulations with and without cation exchanges lead to similar results as far as thermodynamic properties are concerned. From the structural point of view, the MC simulations with cation exchanges give a better description. Owing to these observations, only the results from MC simulations with cation exchanges have been used for further analyses.

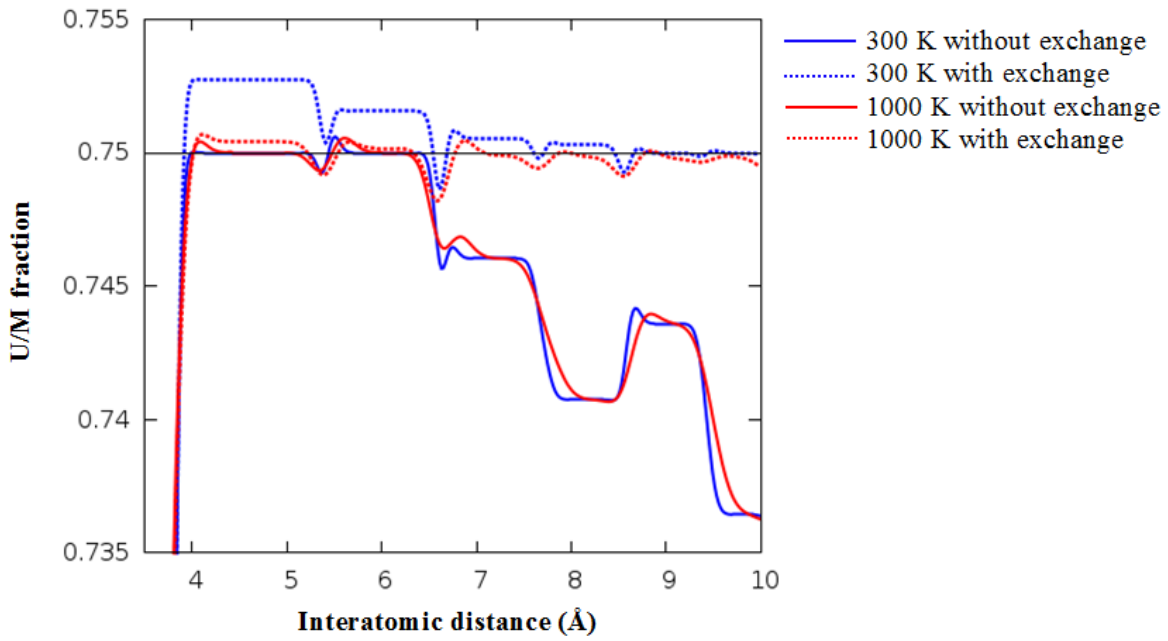

Figure 4: Evolution of U/M (M=U+Pu) fraction in $U_{0.75}Pu_{0.25}O_2$ solid solution at 300 and 1000 K as a function of interatomic distance. The solid lines stand for the simulation without cation exchanges and the dashed lines for the simulations with cation exchanges.

3.4. Deviation from the ideal solid solution as a function of temperature and Pu content

Figure 5 shows the deviation from the ideal solid solution of our systems, i.e. the difference between the calculated number of Pu in the first coordination shell and the expected one as a function of the plutonium content for the whole range of temperatures studied. Note that this deviation is obtained as previously by integrating PDFs in the first coordination shell. For all investigated temperatures, the deviation from the ideal solid solution is very low, with a maximum deviation of 0.11 Pu obtained at 300 K for a Pu content of 37.5 %. Two situations could be observed depending on the temperature which indicates a typical change of the cationic configuration in our systems. At low temperatures (less than ~1800 K) the Pu atoms tended to group together slightly, yielding to a positive cluter deviation, while at high temperatures the Pu atoms tended to separate from each other slightly, leading to a negative deviation. This negative deviation at high temperatures may be due to the predominance of the entropy term in the system, while the enthalpy contribution may be responsible for the clustering observed at lower temperatures. The temperature at which we observed this change of behavior for the cationic distribution varies with the plutonium content. At low Pu contents, the temperature is around 1200 K, while for high Pu contents it is around 2300 K. No relation is established between this phenomenon and experimental observation.

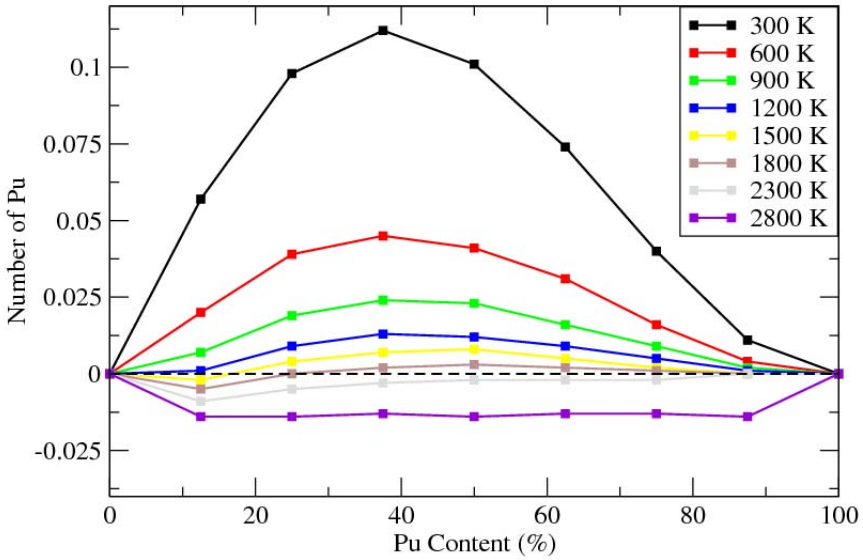

Figure 5: Deviation from the ideal solid solution as a function of plutonium content at different temperatures. This deviation is defined as the difference between the calculated and the expected number of Pu in the first coordination shell.

4. Results and discussions

4.1. Lattice parameter

The lattice parameter of MOX ($U_{1-y}Pu_yO_2$) is computed for various plutonium contents from pure UO_2 to pure PuO_2 in the temperature range from 300 K to the melting temperature. We show in Figure 6.a. the lattice parameter for $U_{1-y}Pu_yO_2$ calculated along with UO_2 Martin's experimental recommendation [39] as well as Shamashita's measurements for PuO_2 [45].

Figure 6.a. shows a regular increase of the lattice parameter of $U_{1-y}Pu_yO_2$ with decreasing plutonium content and increasing temperatures up to the melting point. At room temperature, the computed values of lattice parameters for UO_2 and PuO_2 are 5.469 Å and 5.396 Å respectively. These values are in good agreement with available experimental measurements [45]–[47]. The ionic radius of uranium being slightly larger than that of plutonium, the lattice parameter of UO_2 is as expected higher than that of PuO_2. Furthermore, for all Pu contents, a similar evolution of the lattice parameter with temperature is obtained. This variation is in good agreement with the experimental UO_2 recommendation from Martin [39] and with the PuO_2 experimental data from Yamashita [45]. These results suggest a similar structural behavior for pure uranium and plutonium oxides and for $U_{1-y}Pu_yO_2$ mixed oxides. Lattice parameter results agree well with the values reported by Ma *et al.* [11] using classical MD for a plutonium content of 25 atoms %.

We also calculated the deviation of the lattice parameter from Vegard's law [48] to check if it is still consistent with a solid solution. Vegard's law states that the lattice parameter of a solid solution varies linearly with the component for all temperature. Following this idea, we have calculated the lattice parameter of the mixed oxide as a function of the plutonium content from the lattice parameters of pure UO_2 and pure PuO_2 as suggested by the Vegard's law. The lattice parameter thus obtained is

subtracted to the corresponding value calculated in our simulations in order to calculate the deviation from the Vegard's law.

Figure 6.b shows this deviation as a function of temperature for various plutonium contents. The results highlight that for temperatures ranging from 300 K to 2000 K, the Vegard's law is respected with a slight deviation of around 0.02%. At higher temperatures, the deviation from the Vegard's law increases up to a maximum value of 0.08% around 2600 K. This behavior at high temperatures is related to the Bredig transition and is further investigated in the next section.

Figure 6.c shows the mixing molar volumes as a function of Pu content at different temperatures. As shown in this figure, the mixing molar volumes are very low for all temperatures and Pu contents (with a maximum achieved at 50 % of Pu content). This result is in agreement with the small deviation from Vegard's law reported above and confirms the existence of the ideal solid solution. However, a slight deviation from ideality is more important at high temperatures (3100 K).

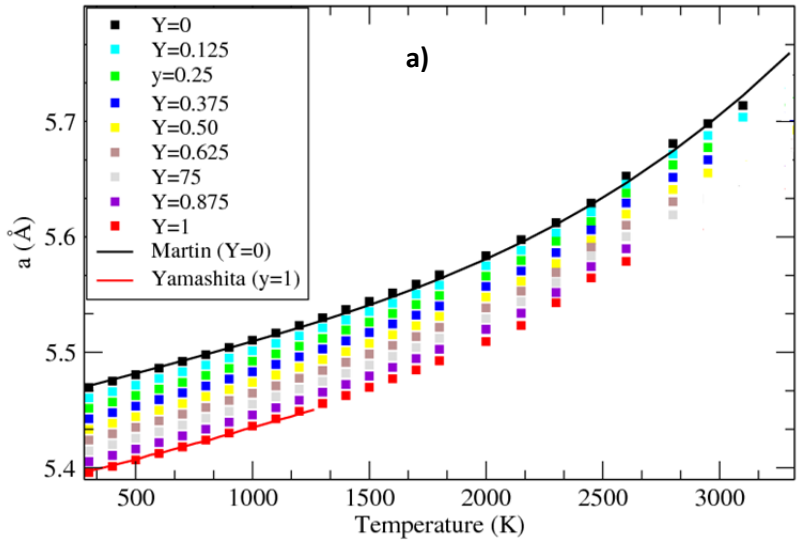

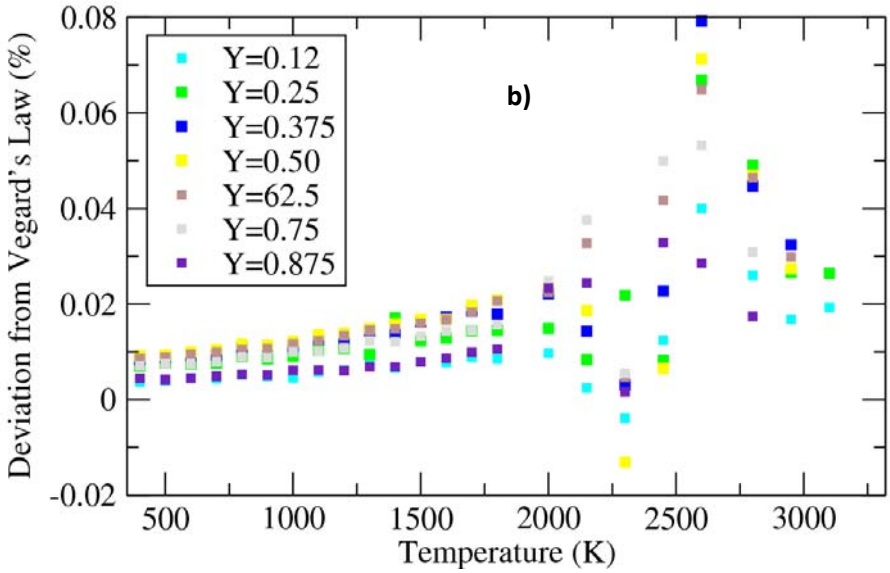

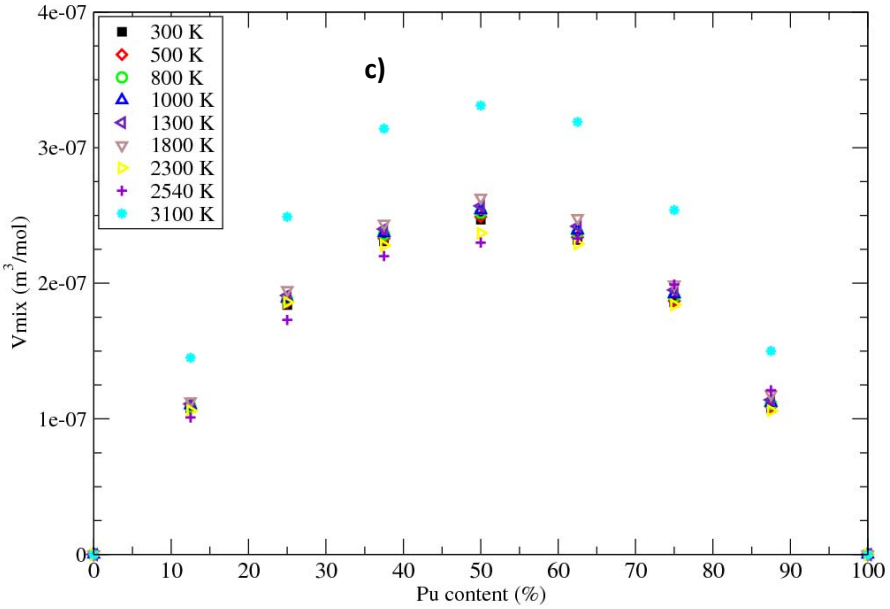

Figure 6: Lattice parameter a), deviation from the Vegard's law b), and mixing volume c) calculated in this work for different temperatures and different plutonium contents in $U_{1-y}Pu_yO_2$. Lattice parameters are compared to both experimental UO_2 Martin's recommendation (solid black line) and experimental Yamashita's PuO_2 data (solid red line). The error bars calculated from the block averaging method (see ref. [49] for details) are too small to be seen (about $7x10^{-9}$ Å).

4.2. Linear thermal expansion coefficient

To further investigate the effect of temperature on expansion, the linear thermal expansion coefficient (α) is evaluated as the first derivative of the lattice parameter with respect to the temperature, as follows.

$$\boldsymbol{\alpha = \frac{1}{a_0}\left(\frac{\partial a}{\partial T}\right)_p} \qquad \text{Eq. 4.1}$$

where a_0 stands for the lattice parameter at 300 K. In our Monte Carlo simulations, we computed the thermal expansion by analyzing volume fluctuations, as shown in equation (Eq.4.2) [50].

$$\boldsymbol{\alpha = \frac{1}{3\langle V\rangle}\left(\frac{\partial\langle V\rangle}{\partial T}\right)_p = \frac{1}{3\langle V\rangle kT^2}\left(\langle V\widehat{H}\rangle - \langle V\rangle\langle\widehat{H}\rangle\right)} \qquad \text{Eq. 4.2}$$

where V is the volume of the system, $\widehat{H}$ is the configurational enthalpy, $\widehat{H}=U+PV$ where U is the intermolecular potential energy.

Figure 7 shows the linear thermal expansion coefficients obtained for various plutonium contents of stoichiometric $U_{1-y}Pu_yO_2$. The comparison is made with the experimental recommendations by Fink for UO_2 [2] and by Uchida for UO_2 and PuO_2 [51]. The linear thermal expansion coefficient evolved with temperature following approximately a similar trend, whatever the plutonium content. Two main regions appear in this graph. The first region concerns temperatures ranging from 300 K to 2300 K, where α values are similar and display a regular evolution for all plutonium contents. The tendency in

this region is consistent with previous theoretical studies [15], [16], [31]. Also, our MC values for α agrees well with Uchida's experimental data for pure UO_2 and PuO_2 [51], with Fahey *et al.* [52] experimental results and with Martin's experimental recommendation on UO_2 [39]. Investigations by Fahey *et al.* showed that at room temperature the α values of different actinide dioxides are almost the same, around 8.5×10^{-6} K^{-1}. This result was expected since the lattice parameters of UO_2, PuO_2 and MOX fuel are close to each other up to ~2300 K [39], [53]–[55] and increase regularly with temperature in this range. This behaviour is confirmed by several other X-ray measurements and theoretical works (see Refs. [15], [31], [39], [45], [53], [55], [56]).

In the second region, which concerns temperatures from 2300 K to the melting temperature, the α values vary from one Pu content to another and increase significantly with temperature up to a maximum before decreasing, forming peaks that appear at different temperatures for each plutonium content. Our results exhibit a discrepancy with Fink's recommendation in this region for all plutonium contents. Fink's recommendation however is based only on UO_2 data. Furthermore, the data used to build the recommendation were scarce and scattered above 2500 K. Therefore, this recommendation should be considered with caution concerning $(U,Pu)O_2$ oxides. Our results are on the contrary in good agreement with Molecular Dynamics simulations results by both Cooper *et al.* [57] and Balboa *et al.* [15]. This behavior of α in the high temperature region may be related to the already mentioned Bredig transition which occurs at the temperature designated T_λ (see next section for more details).

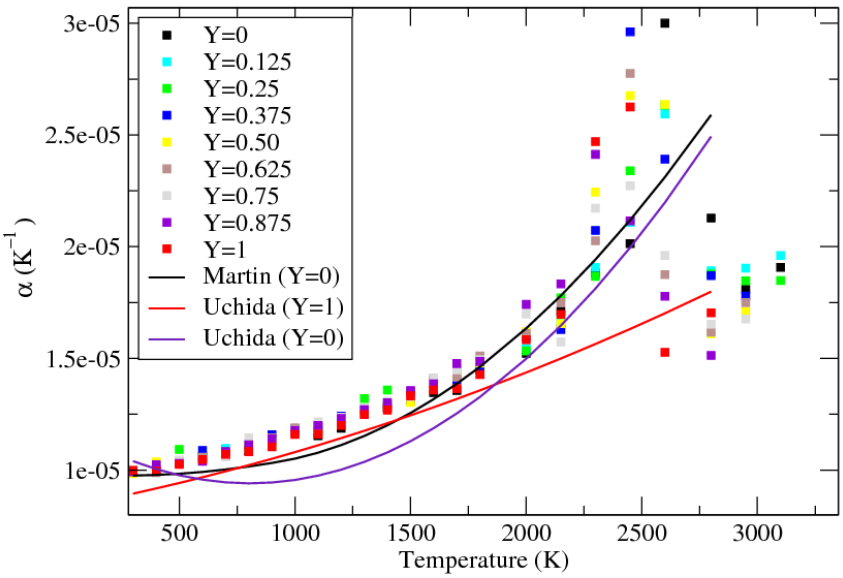

Figure 7: Monte Carlo simulation of the evolution of the linear thermal expansion coefficient as a function of temperature for various plutonium contents in $U_{1-y}Pu_yO_2$ solid solution along with experimental Uchida's data for pure UO_2 and PuO_2 [51] and Martin's recommendation for pure UO_2 [39]. The error bars calculated from the block averaging method (see ref. [49] for details) are too small to be seen (about 3×10^{-6} K^{-1}).

4.3. Enthalpy and specific heat

It is commonly observed that some crystalline materials exhibit significant molecular mobility above a specific onset temperature [58], [59], termed "Tammann temperature", corresponding to a factor of

around 2/3 of the melting temperature. This specific onset temperature has been identified in superionic materials. In regard to UO_2, MD studies [60]–[62] show a significant oxygen disorder at temperatures above 2000 K in agreement with neutron scattering experiments [63]–[66]. These temperatures also acknowledge a change of the material dynamics from that of a "simple" crystal to some kind of highly defective crystalline structure. Ronchi *et al*. [4], Hiernaut *et al*. [67], Hyland *et al*. [68] and most recently Pavlov *et al*. [69] made reasonably accurate measurements of heat capacity of UO_2 using laser flash method in the temperature range including the onset temperature. Their measurements showed peaks around T_λ =2600 K that arose from the second-order transition presented before, and commonly called the "Bredig transition". Nevertheless, this transition is difficult to observe experimentally for UO_2, PuO_2 or MOX. The value of the transition temperature for a given sample is related to its O/M ratio, and due to the variation of O/M ratio during the observation, it often appears that the transition is not clearly seen when increasing the temperature. These technical difficulties lead to high scattering of heat capacity measurements around T_λ; consequently the available recommendations in the literature failed to reproduce the peak related to the Bredig transition.

In the literature, two different interpretations have been attributed to the mechanism behind the Bredig transition. Some authors [16], [69], [70] attributed the increase of the heat capacity to the formation of lattice and electronic defects with the main contribution from Frenkel pair defects. However, the decrease of the heat capacity after the Bredig transition remains unclear up to date. In parallel, other authors [62], [71] have attributed the Bredig transition to the pre-melting of the oxygen sublattice. Zhang *et al*. [71] recently performed a detailed study on superionic UO_2 showing that the peaks related to the Bredig transition could be attributed to the significant mobility of the oxygen ions. According to Zhang *et al*. [21], the thermal motion of the oxygen ions causes high pressure on the U ions. Therefore, the material exhibits some structural rearrangements (by interpenetrating U and O lattices) to accommodate the high internal stresses instead of undergoing the crystal melting. Thus, the oxygen sublattice behaves like a liquid. The latter mechanism proposed since the analysis of the oxygen sublattice around the Bredig transition shows several similarities with what is observed in glass-forming liquids [72], [73]. In this context, our calculated enthalpies and heat capacities appear particularly relevant.

The computed enthalpy increment *i.e.* H(T) – H(300 K) of stoichiometric $U_{1-y}Pu_yO_2$ is displayed in Figure 8.a as well as the UO_2 and PuO_2 experimental Fink's recommendations [2] as well as experimental measurements by Kandan *et al*. [41] for three plutonium contents (21 %, 28 %, and 40 %). As mentioned before, the enthalpy is defined as $H = U + PV = \frac{9}{2} * RT + Uconf + PV$. Where U, P, and V are respectively the energy, the pressure and the volume of the system. The energy U can also be written as the sum of the configurational energy of the system Uconf (the energy coming from the CRG potential) and a perfect gas (or kinetic) contribution equal to $\frac{9}{2} * RT$ (corresponding to the energy of an isolated UO_2 molecule). The calculated results are in good agreement with PuO_2 Fink's recommendation up to 1000 K and UO_2 Fink's recommendation up to 2650 K. For the whole range of investigated temperatures, the calculated enthalpy increments are identical for all plutonium contents and increased approximately linearly with increasing temperature even if the points around 2300 K are slightly scattered. This scattering was also observed by Potashnikov *et al*. [16] in the range 2000-2600 K and attributed to the first-order phase transition due to the anionic sublattice instability. Although our results did not fit well with the Fink's PuO_2 recommendation above 1000 K, they are in agreement with the experimental calorimetric measurements of Kandan *et al*. [41]. The study by Kandan *et al*. indicated that the enthalpy increment values for the three investigated compositions

(21%, 28%, and 40%) are indistinguishable within the experimental uncertainties. Furthermore, recent theoretical works showed that there is no noticeable influence of the plutonium content on the enthalpy increment of MOX solid solution [15], [31] below the melting point. This result is not in agreement with the Fink's recommendation, which suggests two different behaviors for UO_2 and PuO_2. Nevertheless, Fink highlights in his article that few data on PuO_2 were available at this time especially at high temperatures compared to UO_2.

Figure 8.b shows the mixing molar enthalpies as a function of plutonium content. The obtained values obtained are minimal for all Pu contents up to 1800 K. This is the expected behavior for an ideal solution, and consistent with the fact that the ionic radii of U and Pu are close to each other [74]. Above 1800 K, the mixing enthalpies are small but significantly negative at 2300 K and 2450 K, with a minimum achieved at 50 % of Pu content, while at 3100 K the mixing enthalpy goes back to values close to zero. This behavior at high temperature may be related to the Bredig transition.

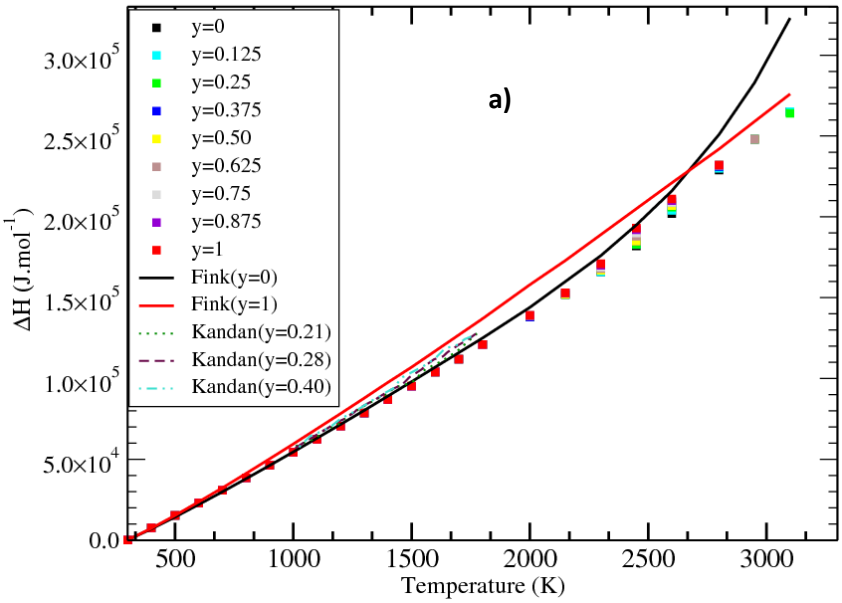

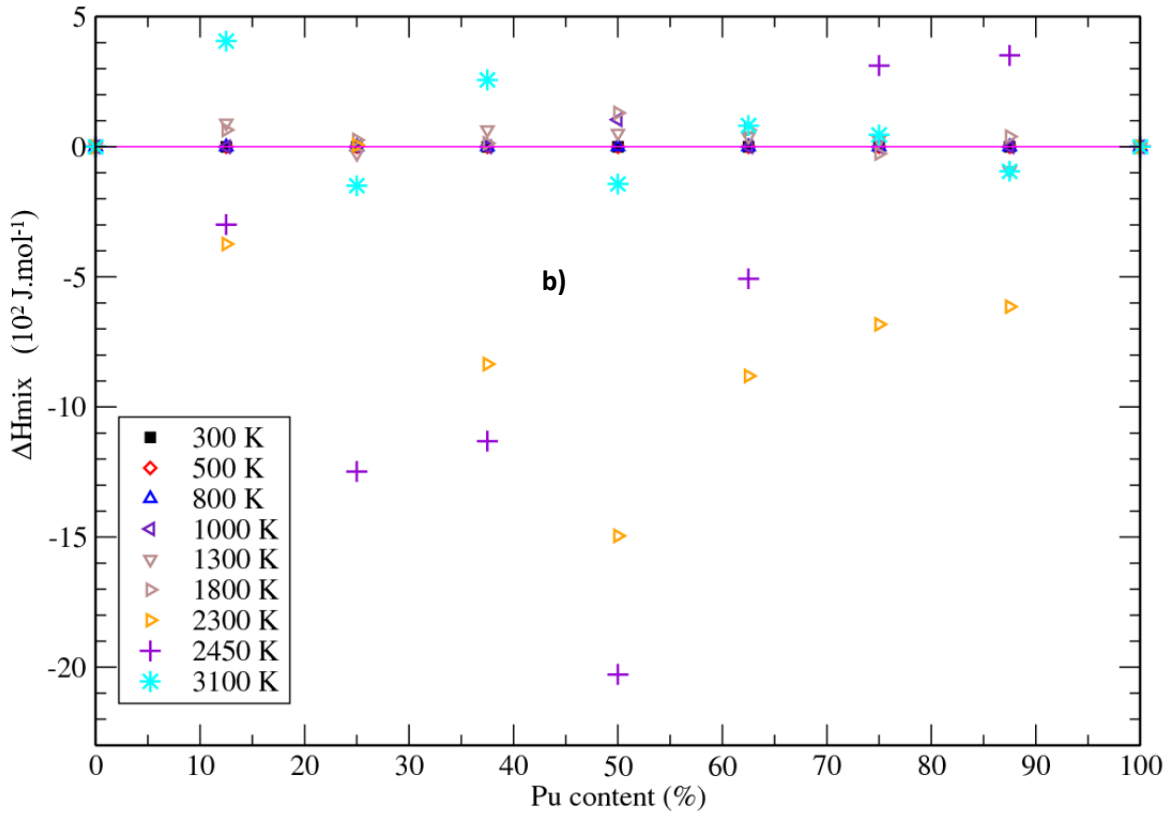

Figure 8: Monte Carlo results of the evolution of the enthalpy increment as a function of temperature for different plutonium contents in $U_{1-y}Pu_yO_2$ solid solution a) and mixing enthalpy as a function of Pu content b). The results are compared to experimental UO_2 and PuO_2 Fink's recommendation data [75] as well as experimental measurements by Kandan *et al.* [23] for three different plutonium contents, namely 21 %, 28 %, and 40 %. The error bars calculated from the block averaging method (see ref. [49] for details) are too small to be seen (about $3x10^{-3}$ $J.mol^{-1}$).

The heat capacity of MOX fuel is a fundamental property that governs nuclear reactor performance and safety. Its knowledge is essential for fuel performance codes. Heat capacity is the first derivative of the enthalpy with respect to the temperature at constant pressure (as shown by equation Eq.4.3). So, compared to enthalpy increment, more precise information can be extracted from the analysis of the heat capacity.

$$C_p = \left(\frac{\partial H}{\partial T}\right)_p \qquad \text{Eq. 4.3}$$

We evaluated the heat capacity using two different approaches that we call here "*indirect*" and "*direct*". In the indirect approach, the previous results of the variation of enthalpy displayed in Figure 8 are fitted using the exponential form as the one proposed by Fink to build its recommendation (see Eq.4.4 and ref [75] for details). Then the heat capacity is calculated as the analytical derivative of the fitting function. This approach is commonly used by experimentalists to post-treat their increment enthalpy measurements and was used by Fink to build its recommendations. It was also used by Cooper *et al.* [17] to determine the heat capacity of pure oxides as UO_2, ThO_2 and PuO_2 using classical MD. The value of C_p obtained by this approach is strongly conditioned by the mathematical form chosen to fit ΔH. Moreover, the fitted parameters may considerably vary from one compound to another and have no physical meaning. Our results using the indirect approach are displayed in

Figure 9.c along with UO_2 and PuO_2 Fink's recommendations [75]. The fits are made for temperatures up to 2200 K because, above this temperature, they were clearly inappropriate. For all plutonium contents (except pure PuO_2), a good agreement with UO_2 Fink's recommendation is found up to 2200 K. Note that this empirical approach well reproduces the form of UO_2 Fink's recommendation but failed for PuO_2. Again, Fink highlights in his article that at this time very few heat capacity data on PuO_2 were available, especially at high temperatures (more than 298.15 K) to validate the PuO_2 recommendation. A more recent recommendation by Konings *et al*. [76] shows the same trend of heat capacity for both UO_2 and PuO_2.

$$\Delta \mathbf{H} = \boldsymbol{C_1\theta}\left[\left(\boldsymbol{e^{\theta/T}-1}\right)^{-1} - \left(\boldsymbol{e^{298{,}15/T}-1}\right)^{-1}\right] + \boldsymbol{C_2}\left[\boldsymbol{T^2 - (298,15)^2}\right] + \boldsymbol{C_3 e^{-E_a/T}} \quad \text{Eq. 4.4}$$

In the second approach, the direct one, the heat capacity is computed by analyzing the fluctuations of the energy during a Monte Carlo simulation. As already pointed by Jorgensen *et al.* [77], the heat capacity has to be separated into two contributions residual and ideal parts. The ideal part can be considered as constant above the Debye temperature (about 377 K and 425 K for UO_2 and PuO_2 respectively [78]) and obtained by considering the compound as an ideal gas. The ideal heat capacity used in this work is assumed identical for all systems and equal to 20.786 J/mol/K. The residual part is computed from the following equation. The partial derivatives that appear in this equation are calculated using the fluctuation formula presented in Equation Eq.4.5. More details on this computational method are available in ref. [50].

$$\boldsymbol{C_p^{res}(T,P)} = \left(\frac{\partial\langle U\rangle}{\partial T}\right)_{\boldsymbol{p}} + \boldsymbol{P}\left(\frac{\partial\langle V\rangle}{\partial T}\right)_{\boldsymbol{p}} - \boldsymbol{Nk} = \frac{\mathbf{1}}{\boldsymbol{kT^2}}\left(\langle \boldsymbol{U\widehat{H}}\rangle - \langle \boldsymbol{U}\rangle\langle \boldsymbol{\widehat{H}}\rangle\right) + \frac{\boldsymbol{P}}{\boldsymbol{kT^2}}\left(\langle \boldsymbol{V\widehat{H}}\rangle - \langle \boldsymbol{V}\rangle\langle \boldsymbol{\widehat{H}}\rangle\right) - \boldsymbol{Nk}$$

Eq. 4.5

Figure 9.a shows our direct computed UO_2 heat capacity as a function of temperature together with experimental data [4], [69], [79], thermodynamic $(U,Pu)O_2$ model by Gueneau *et al.,* [80] using CALPHAD method, Fink's recommendation [75] and a recent model proposed by *Pavlovet al*. [69]. Below 2000 K, all curves have almost the same trend (slight variation of heat capacity). Above 2000 K, the curves may be divided into two groups. A first group, including the Fink's recommendation [75] and the thermodynamic $(U,Pu)O_2$ model by Gueneau *et al.* [80], shows an increase of the heat capacity up to the melting temperature. A second group, including experimental data [4], [69], [79], the model proposed by Pavlov *et al*. [69] and our calculations, shows a peak around 2600 K.

Figure 9.b shows the direct computed $U_{1-y}Pu_yO_2$ heat capacity as a function of temperature along with Fink's UO_2 and PuO_2 recommendation [75] and thermodynamic model proposed by Gueneau *et al*., [80] using the CALPHAD method. For all plutonium contents, the calculated data have the same trend and the same behavior as previously observed in section 4.2 for the linear thermal expansion coefficient. Below 2000 K, heat capacity followed a gradual increase and took the same values for all plutonium contents. Above 2000 K, a much more rapid increase is observed and could be attributed to the enthalpy required to create the oxygen disorder. The signature of this phenomenon was already observed in Figure 7 showing the linear thermal expansion coefficient. The observed peaks, referred to as λ-peaks, were discovered and characterized for the first time by Bredig *et al*. [3] for most of the compounds presenting a fluorite-type structure. This is the main signature of the second-order phase transition, also called *"diffusing phase transition*" or *"superionic transition*". A superionic conductor behavior is attributed to the material above this transition. Figure 10 shows the pair distribution

functions (PDF) of the oxygen-oxygen (O-O) distances and plutonium-plutonium (Pu-Pu) in stoichiometric $U_{0.75}Pu_{0.25}O_2$ for various temperatures. The O-O PDF is very sensitive to the increase of temperature, which leads to the rapid broadening of the peaks of the O-O PDF compared to the Pu-Pu one. At temperatures up to 900 K, the PDF decreases to zero for both O-O and Pu-Pu between the first and second coordination shells (after the first peak, ie after $r = 3.25$ Å and $r = 4.80$ Å for O-O and Pu-Pu PDF, respectively). Above 900 K, the O-O PDF no longer decreases to zero after the first peak while it is still the case for the Pu-Pu PDF at up to 2600 K. This means that the fluctuations in the oxygen sublattice are sufficiently large to enable the oxygen atoms to move from one site to another. Zhang *et al*. [71] showed that oxygen ions preferentially hop between sites having multiples of the interatomic distance, a behavior observed in many glass-forming liquids. At 2600 K and 3300 K for O-O and Pu-Pu respectively, the second peak of the PDF almost disappeares. This behavior corresponds to the liquid character of the oxygen and plutonium sublattices respectively. The liquid character of the oxygen sublattice corresponds to a pre-melting step, which starts at the Bredig transition, while the liquid character of the plutonium sublattice appears after the melting temperature of the compound.

As shown previously [31], the superionic transition is closely related to the creation of oxygen defects and to the increase of the self diffusivity of oxygen ions [12], causing a "bump" in several properties as linear thermal expansion coefficient, enthalpy and heat capacity. Potashnikov *et al*. [16] also associated this manifestation of λ-peaks to the saturation in anti-Frenkel defects, which corresponds to a maximal disorder in the anion sublattice. From our thermal expansion and heat capacity results, this transition is found to occur at 2600 K and 2300 K for UO_2 and PuO_2 respectively, corresponding to a temperature equal to 0.85 times the melting temperatures of UO_2 and PuO_2 which are 3120 K [81] and 3040 K [82] respectively. These results are consistent with previous experimental [4], [83] and theoretical [15], [16], [31], [84]–[86] works showing that the Bredig's transition occurs around 0.8 times the melting temperature in various actinide oxides. Our studies are in agreement with other theoretical studies showing the existence of Bredig's transition for all Pu contents including PuO_2. However even if this transition is well established in UO_2 and ThO_2 pure oxides as well as in $(U_{1-y}Pu_y)O_2$ and $(U_{1-y}Th_y)O_2$ mixed oxides no experimental results neither recommendations predicted the Bredig's transition in PuO_2 except that of Konings *et al*. [76]. A recent study on antifluorite Li_2O by Lavrentiev *et al*. [87] shows that the heat capacity of this material rises all the way up to the melting point, where it abruptly falls down. This sudden drop is therefore different from the progressive return to normal behavior observed in the fluorite type structure.

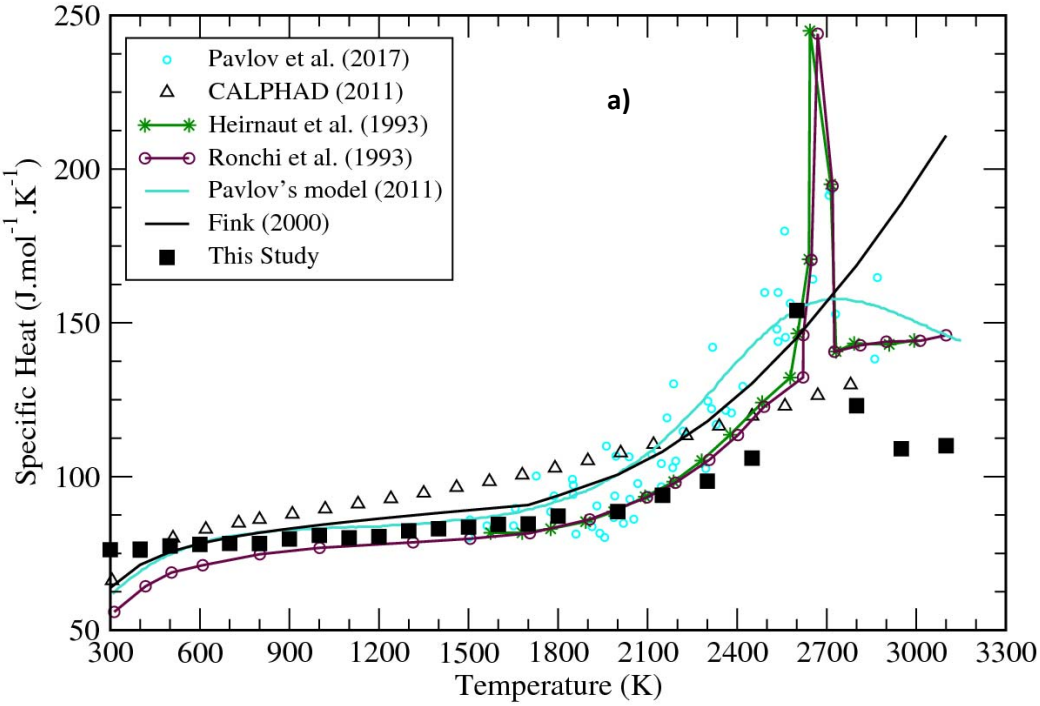
a)
Pavlov et al. (2017)
CALPHAD (2011)
Heirnaut et al. (1993)
Ronchi et al. (1993)
Pavlov's model (2011)
Fink (2000)
This Study
Specific Heat (J.mol^{-1}.K^{-1})
Temperature (K)
250
200
150
100
50
300
600
900
1200
1500
1800
2100
2400
2700
3000
3300

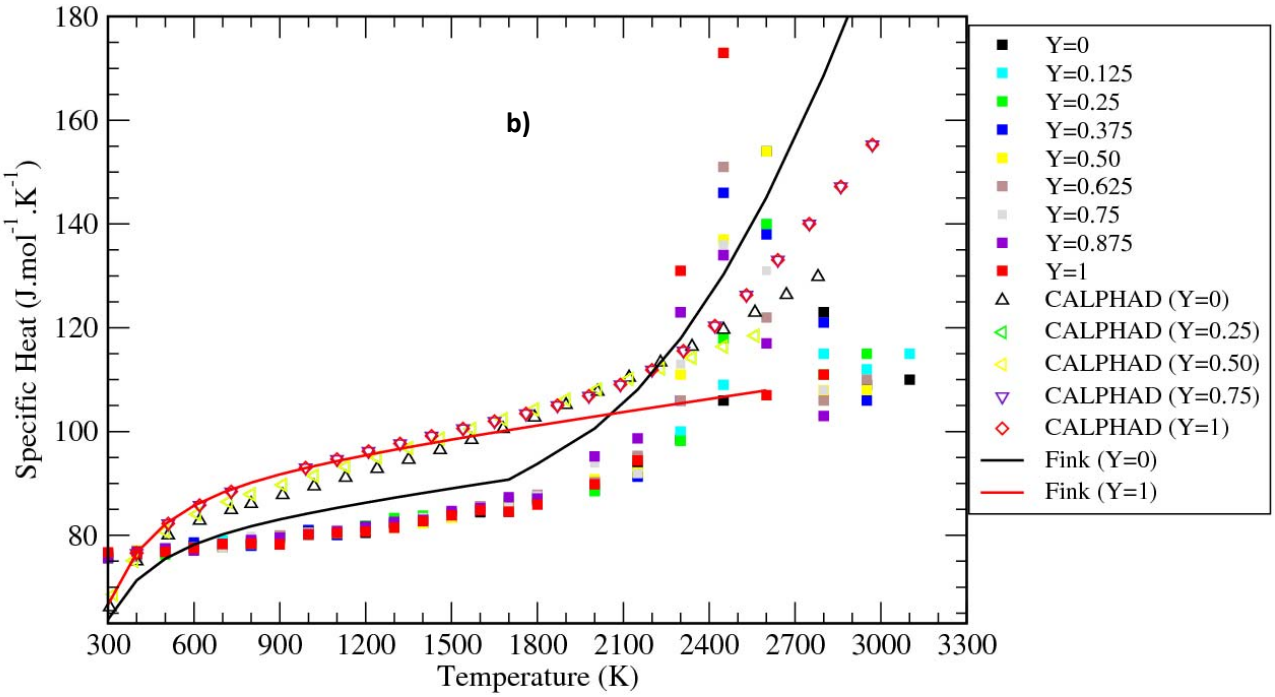
b)
Y=0
Y=0.125
Y=0.25
Y=0.375
Y=0.50
Y=0.625
Y=0.75
Y=0.875
Y=1
CALPHAD (Y=0)
CALPHAD (Y=0.25)
CALPHAD (Y=0.50)
CALPHAD (Y=0.75)
CALPHAD (Y=1)
Fink (Y=0)
Fink (Y=1)
Specific Heat (J.mol^{-1}.K^{-1})
Temperature (K)
180
160
140
120
100
80
300
600
900
1200
1500
1800
2100
2400
2700
3000
3300

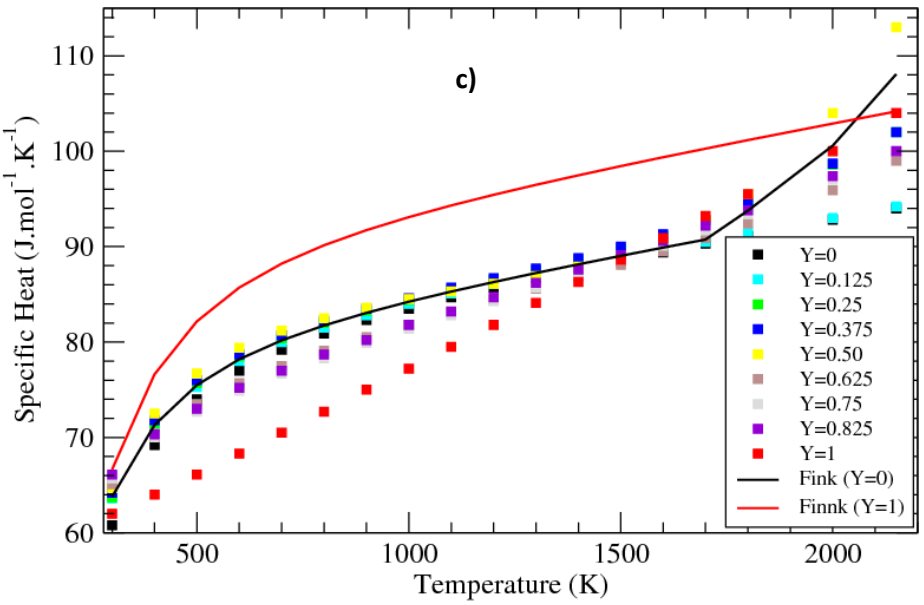

Figure 9: Evolution with temperature of UO_2 a) and $U_{1-y}Pu_yO_2$ b) heat capacity using the direct method and indirect calculation of $U_{1-y}Pu_yO_2$ heat capacity c). The results are compared with experimental UO_2 data (Ronchi *et al.* [4], Heirnaut *et al.* [67], Pavlov *et al.* [69]), Pavlov's model [69], Fink's recommendations [75], and thermodynamic model proposed by Gueneau *et al.* [80] using CALPHAD method. For our results, the error bars calculated from the block averaging method (see ref. [49] for details) are about 4 $J.mol^{-1}.K^{-1}$.

The heat capacity calculated in this work using the direct method and displayed in Figure 9.b does not match the Fink's recommendations. Below 500 K, the recommendation shows a rapid rise, which cannot be reproduced in classical MC and MD simulations due to the non-consideration of quantum mechanic effects in these calculations. Nevertheless, this part of the curve can be obtained theoretically from phonon spectrum calculations. From 800 K to 2000 K, Figure 9.b shows an underestimation about 4 $J.mol^{-1}.K^{-1}$ in computed heat capacity compared to the Fink's UO_2 recommendation for all plutonium contents. However, the thermodynamic $(U,Pu)O_2$ model by Gueneau *et al.* [80] using the CALPHAD method slightly overestimated this recommendation and showed a slight effect of Pu content. The underestimation observed in our calculations is on the order of magnitude of the calculated statistical error. Theoretically, heat capacity of actinide oxide and mixed oxide can be considered as the sum of several terms: heat capacity at constant volume C_V, at which can be added a dilatation term C_d, a Schottky term C_{Sch} and a Frenkel term C_F. Kato *et al.* [88] showed that it is important to analyze the C_{Sch} and C_F terms in heat capacity of PuO_2. An increasing PuO_2 heat capacity of about 10 $J.mol^{-1}.K^{-1}$ when the temperature goes from 400 K to 1000 K as well as a rapid growth for temperatures above 1500 K has been observed adding C_{Sch} and C_F terms. Several authors [89]–[91] showed that adding the Schottky term to the PuO_2 heat capacity resulted in values closer to the experimental Oetting's data [92]. Unfortunately, C_{Sch} and C_F terms can not be evaluated in our MC simulations and this could be the cause of the slight underestimation of our calculated heat capacity from 800 K to 2000 K. Contribution of electronic and Schottky defects on heat capacity as a function of temperature can be evaluated using empirical formula proposed in refs [13], [93]. Contrary to Fink's recommendation, our calculations show a return to normal behaviour after the Bredig transition. This transition is responsible for the peak observed in our simulations around 2300 K while the Fink's recommendation suggested a rapid and continuous increase of the

heat capacity. This difference with UO_2 Fink's recommendation is probably due to the use of an exponential form to fit ΔH experimental data though these data showed almost a linear evolution with temperature.

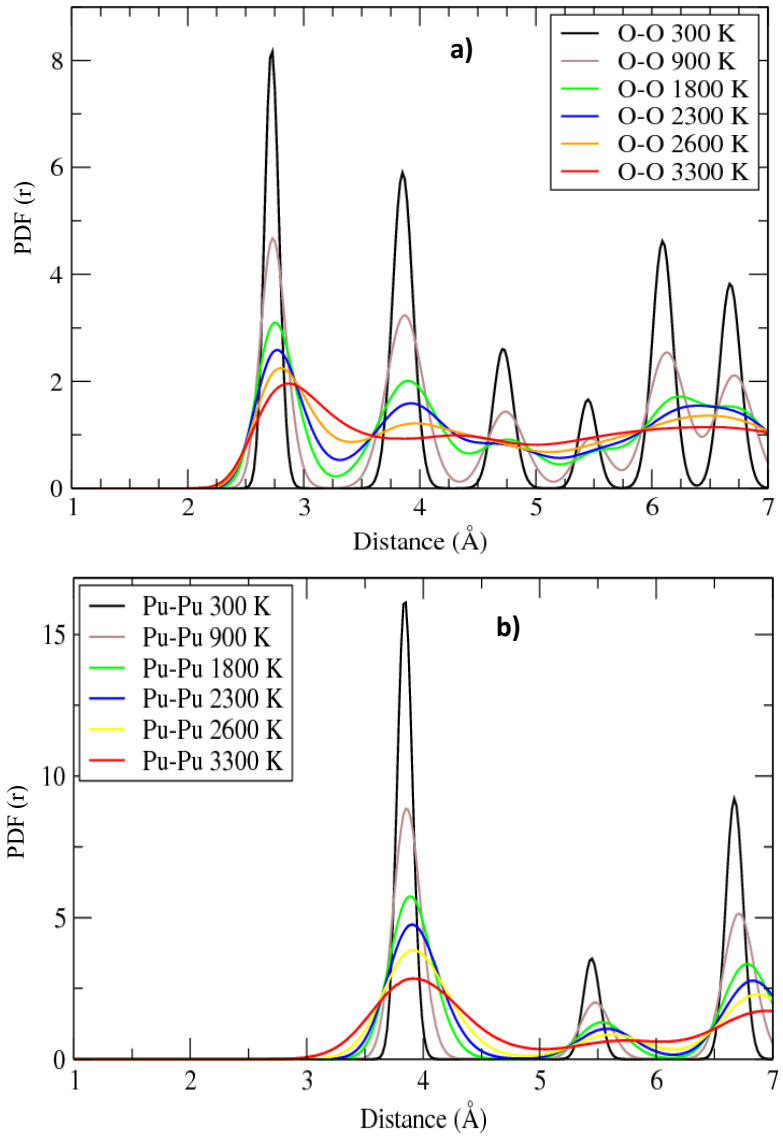

Figure 10: Pair distribution functions (PDF) of the oxygen sublattice (oxygen-oxygen) a) and of the cation sublattice (plutonium-plutonium) b) as a function of the pair distance in the stoichiometric $U_{0.75}Pu_{0.25}O_2$ at different temperatures.

4.4. Bulk modulus

The bulk modulus B, which is the inverse of the compressibility coefficient β_T, can be obtained from the simulations in the NPT ensemble by evaluating the evolution of the volume of the system as a function of pressure at constant temperature. In our Monte Carlo simulations, this property is computed from volume fluctuations, as given in equation Eq.4.6 [50].

$$\frac{1}{B} = \beta_T = -\frac{1}{\langle V \rangle}\left(\frac{\partial \langle V \rangle}{\partial P}\right)_T = \frac{1}{\langle V \rangle kT}\left(\langle V^2 \rangle - \langle V \rangle^2\right) \qquad \text{Eq. 4.6}$$

The computed bulk moduli of UO_2 and PuO_2 at room temperature are listed in Table 5. We compare our values with both MD and *ab initio* studies as well as with available experimental data. Our results are in agreement with *ab initio* calculations and showed that the bulk modulus of UO_2 is lower than the one of PuO_2, whereas MD simulations using CRG potential and experimental results exhibit the opposite behavior. A good agreement is found between our calculated bulk modulus of UO_2 and the experimental data of Idiri [94]. For PuO_2, the difference between our calculated value and the experimental one from Idiri [94] is around 19 %. However, there were some significant discrepancies between reported experimental values for PuO_2 [94] (ranging from 178.0 GPa to 379.0 GPa); thus, it is difficult to conclude on the quantitative quality of our calculated results.

The bulk modulus of $U_{1-y}Pu_yO_2$ for all plutonium contents is computed and plotted in Figure 11 together with the experimental UO_2 data of Browning [95] and the ESNII+ recommendation [96]. Figure 11 shows that for the entire range of plutonium content, the bulk modulus decreases linearly with the temperature up to ~2600 K. At 2300 K, in the region of the Bredig's transition, we observe a small kink that leads to an increase of the bulk modulus and causes a discontinuity. This tendency is consistent with Browning's experimental work on UO_2 [95] and with some MD simulation results [9], [11], [15], [97]. Furthermore, our results fitted well with the recommendation of ESNII+ European catalog [96]. According to Cooper *et al*. [17], actinide oxides (AmO_2, CeO_2, CmO_2, NpO_2, ThO_2, PuO_2, UO_2) exhibit a roughly linear dependence of the bulk modulus with temperature. This reflects the decrease of the bulk modulus with increasing lattice parameter. Our results did not show any effect of the plutonium content on bulk modulus as recommended in the ESNII+ European catalogue [96]. Even if bulk modulus measurements as a function of the content are not available in the literature, only a moderate increase in Young's modulus with the addition of plutonium content has been reported by some authors. Novion *et al*. [98] results indicated that the Young's modulus increases by 4% when the plutonium content is raised from 0 to 15%, while Nutt *et al*. [99] found an only 11% higher modulus value for a mixed (U, Pu)O_2 containing 70% plutonium.

For high temperatures, since no recommendation is given over the temperature range 2900 - 3100 K, it is difficult to conclude unequivocally. Therefore, our results above 2600 K constitute reliable predictions.

Table 5. The bulk modulus of UO_2 and PuO_2 computed at 300 K using MC simulation with cation exchanges. These results are compared to the other theoretical *ab initio,* and MD works as well as experimental data available in literature.

	Bulk modulus (GPa)			
	MC	MD	*Ab initio*	Experimental
UO_2	207	226.01[b]	196[a]	207[c]
PuO_2	212	220.80[b]	199[a]	178[c]

[a]ref [25]. [b]ref [17]. [c]ref [94].

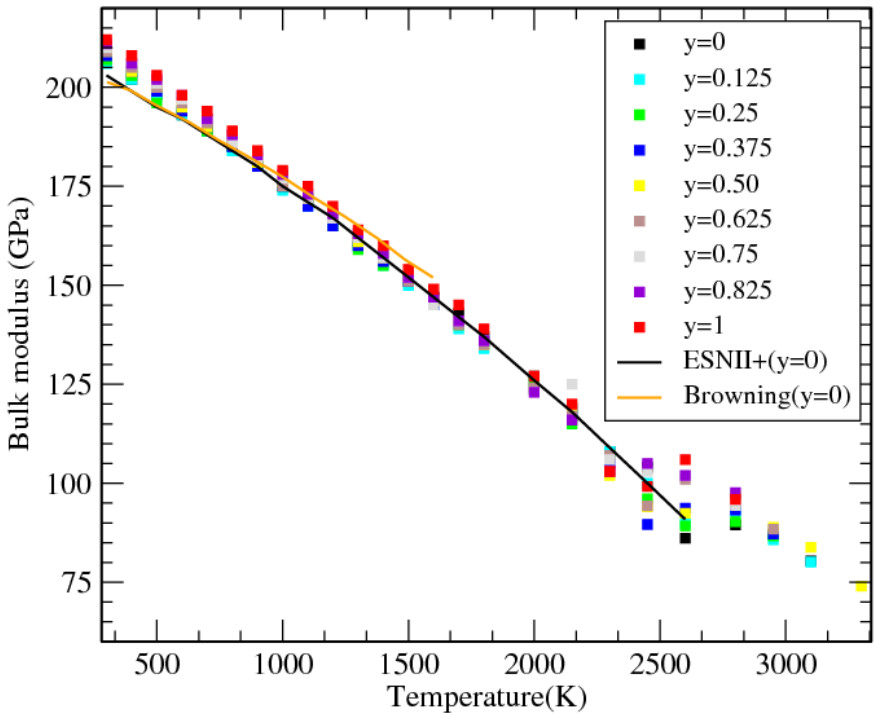

Figure 11: Monte Carlo simulation of the bulk modulus as a function of temperature for different plutonium contents in $U_{1-y}Pu_yO_2$ solid solution along with ESNII+ recommendation [37] and Browning's experimental data [36]. The error bars calculated from block averaging method (see ref. [49] for details) are about 5 GPa.

5. Conclusion

The lattice parameter, the enthalpy, the linear thermal expansion coefficient, the bulk modulus, and the specific heat of stoichiometric $U_{1-y}Pu_yO_2$ MOX fuel is investigated from 300 K to the melting temperature in the whole range of plutonium contents from pure UO_2 to pure PuO_2 using MC simulations using the CRG empirical potential. A specific MC algorithm is used to allow the investigation of the effect of cation exchange on all investigated properties and their impact on the characteristics of the solid solution. Our results showed that at room temperature, there is no noticeable effect of the cation exchange algorithm on thermodynamic properties, and the obtained results are in good agreement with MD works as well as with experimental data reported in the literature. The difference between the two MC algorithms with and without cation exchanges is visible only on the atomic structures. The cation exchange algorithm yields a random distribution of cations close to what is expected for an ideal solid solution. The study of atomic structure of $U_{0.70}Pu_{0.30}O_2$ by analyzing the tetrahedron distribution around an oxygen atoms as a function of the number of Pu neighbors through MC simulation with cation exchange algorithm is consistent with experimental ^{17}O NMR measurements by Vigier *et al*. [19]. Note that both the experimental and calculated results are close to a theoretical distribution corresponding to an ideal solid solution. This good description of an ideal solid solution is an intrinsic feature of the MC simulation method and could not have been achieved by MD. Concerning thermodynamic properties, our results yielded the same trends as those obtained with the CRG empirical potential using MD method [15], [31]. These results also corroborate Martin and Fink's recommendations at up to 2300 K especially for UO_2. A Bredig transition is detected at 0.85xTm (Tm being the melting temperature) and is particularly

visible on the curves showing the evolution with temperature of the linear thermal expansion coefficient and the heat capacity for all Pu contents including PuO_2. We also showed that the indirect calculation of the specific heat (by fitting enthalpy results with the mathematical form used in the Fink's recommendation) is close to UO_2 Fink's recommendation, but questions have been raised concerning the physical reality of these results. Our direct calculations of the specific heat (by analysing the energy fluctuations within MC simulations) predicted a return to normal behavior after the Bredig transition as obtained experimentally by Ronchi *et al*. [4]. This return to normal behavior can not be reproduced by the exponential functions used by Fink to establish its recommendations. The results obtained in this work underline the need for a reassessment at high temperature of the empirical recommendations commonly used to address thermodynamic properties of uranium and plutonium oxides.

Acknowledgements

This work was performed using the GIBBS code co-developed by IFPEN, Paris-Sud University and CNRS. High-performance resources from Grand Equipement National de Calcul Intensif (GENCI) [Centre Commun de recherche et Technologie (CCRT)] were used for this investigation. The authors wish to express their gratitude to J. Léchelle, D. Staicu, P. Martin, N. Chauvin, M. Lainet, G. Jomard, M. Freyss, and M. Bertolus for fruitful discussions. This research is part of the Investigations Supporting MOX Fuel licensing in ESNII Protocol Reactors (INSPYRE) project, which has received funding from Euratom research and training program 2014-2018 under grant 754329.

References

[1] J. J. Carbajo, G. L. Yoder, S. G. Popov, et V. K. Ivanov, « A review of the thermophysical properties of MOX and UO2 fuels », *J. Nucl. Mater.*, vol. 299, n° 3, p. 181‑198, déc. 2001.

[2] J. K. Fink, M. G. Chasanov, et L. Leibowitz, « Thermophysical properties of uranium dioxide », *J. Nucl. Mater.*, vol. 102, n° 1‑2, p. 17‑25, nov. 1981.

[3] A. S. Dworkin et M. A. Bredig, « Diffuse transition and melting in fluorite and antifluorite type of compounds. Heat content of potassium sulfide from 298 to 1260.degree.K », *J. Phys. Chem.*, vol. 72, n° 4, p. 1277‑1281, avr. 1968.

[4] C. Ronchi et G. J. Hyland, « Analysis of recent measurements of the heat capacity of uranium dioxide », *J. Alloys Compd.*, vol. 213‑214, p. 159‑168, oct. 1994.

[5] Faraday M., « Faraday's diary. (eds Martin T). G. Bell and sons, ltd (1932) ».

[6] A. V. Chadwick, « Transport in defective ionic materials: from bulk to nanocrystals », *Phys. Status Solidi A*, vol. 204, n° 3, p. 631‑641, mars 2007.

[7] A. Annamareddy et J. Eapen, « Mobility propagation and dynamic facilitation in superionic conductors », *J. Chem. Phys.*, vol. 143, n° 19, p. 194502, nov. 2015.

[8] Ralph J, Hyland GJ., « Empirical confirmation of a Bredig transition in UO2. J Nucl Mater 132, 76-79 (1985). »

[9] K. Yamada, K. Kurosaki, M. Uno, et S. Yamanaka, « Evaluation of thermal properties of mixed oxide fuel by molecular dynamics », *J. Alloys Compd.*, vol. 307, n° 1‑2, p. 1‑9, juill. 2000.

[10] T. Arima, S. Yamasaki, Y. Inagaki, et K. Idemitsu, « Evaluation of thermal conductivity of hypostoichiometric (U, Pu)O2−x solid solution by molecular dynamics simulation at temperatures up to 2000K », *J. Alloys Compd.*, vol. 415, n° 1‑2, p. 43‑50, mai 2006.

[11] J. Ma, J. Zheng, M. Wan, J. Du, J. Yang, et G. Jiang, « Molecular dynamical study of physical properties of (U0.75Pu0.25)O2−x », *J. Nucl. Mater.*, vol. 452, n° 1‑3, p. 230‑234, sept. 2014.

[12] C. B. Basak et A. S. Kolokol, « A Novel Pseudo-Ion Approach in Classical MD Simulation: A Case Study on (U0.8Pu0.2)O2 Mixed Oxide », *J. Am. Ceram. Soc.*, vol. 95, n° 4, p. 1435‑1439, avr. 2012.
[13] K. Kurosaki, K. Yamada, M. Uno, S. Yamanaka, K. Yamamoto, et T. Namekawa, « Molecular dynamics study of mixed oxide fuel », *J. Nucl. Mater.*, vol. 294, n° 1‑2, p. 160‑167, avr. 2001.
[14] T. Arima, S. Yamasaki, K. Idemitsu, et Y. Inagaki, « Equilibrium and nonequilibrium molecular dynamics simulations of heat conduction in uranium oxide and mixed uranium–plutonium oxide », *J. Nucl. Mater.*, vol. 376, n° 2, p. 139‑145, mai 2008.
[15] H. Balboa, L. Van Brutzel, A. Chartier, et Y. Le Bouar, « Assessment of empirical potential for MOX nuclear fuels and thermomechanical properties », *J. Nucl. Mater.*, vol. 495, p. 67‑77, nov. 2017.
[16] S. I. Potashnikov, A. S. Boyarchenkov, K. A. Nekrasov, et A. Ya. Kupryazhkin, « High-precision molecular dynamics simulation of UO2–PuO2: Pair potentials comparison in UO2 », *J. Nucl. Mater.*, vol. 419, n° 1‑3, p. 217‑225, déc. 2011.
[17] M. W. D. Cooper, M. J. D. Rushton, et R. W. Grimes, « A many-body potential approach to modelling the thermomechanical properties of actinide oxides », *J. Phys. Condens. Matter*, vol. 26, n° 10, p. 105401, mars 2014.
[18] P. Martin *et al.*, « XAS study of (U1−yPuy)O2 solid solutions », *J. Alloys Compd.*, vol. 444‑445, p. 410‑414, oct. 2007.
[19] J.-F. Vigier, P. M. Martin, L. Martel, D. Prieur, A. C. Scheinost, et J. Somers, « Structural Investigation of ($U_{0.7}$ $Pu_{0.3}$)O_{2-x} Mixed Oxides », *Inorg. Chem.*, vol. 54, n° 11, p. 5358‑5365, juin 2015.
[20] N. Metropolis et S. Ulam, « The monte carlo method », *J. Am. Stat. Assoc.*, vol. 44, n° 247, p. 335–341, 1949.
[21] N. L. Allan, G. D. Barrera, M. Yu. Lavrentiev, I. T. Todorov, et J. A. Purton, « Ab initio calculation of phase diagrams of ceramics and minerals », *J. Mater. Chem.*, vol. 11, n° 1, p. 63‑68, 2001.
[22] M. Y. Lavrentiev, N. L. Allan, G. D. Barrera, et J. A. Purton, « Ab Initio Calculation of Phase Diagrams of Oxides », p. 6.
[23] R. Babarao et J. Jiang, « Unprecedentedly High Selective Adsorption of Gas Mixtures in *rho* Zeolite-like Metal−Organic Framework: A Molecular Simulation Study », *J. Am. Chem. Soc.*, vol. 131, n° 32, p. 11417‑11425, août 2009.
[24] A. Sirjoosingh, S. Alavi, et T. K. Woo, « Grand-Canonical Monte Carlo and Molecular-Dynamics Simulations of Carbon-Dioxide and Carbon-Monoxide Adsorption in Zeolitic Imidazolate Framework Materials », *J. Phys. Chem. C*, vol. 114, n° 5, p. 2171‑2178, févr. 2010.
[25] P. S. Ghosh *et al.*, « Melting behavior of (Th,U)O 2 and (Th,Pu)O 2 mixed oxides », *J. Nucl. Mater.*, vol. 479, p. 112‑122, oct. 2016.
[26] C. I. Maxwell et J. Pencer, « Molecular dynamics modelling of the thermal conductivity of off-stoichiometric UO2±x and (UyPu1−y)O2±x using equilibrium molecular dynamics », *Ann. Nucl. Energy*, vol. 131, p. 317‑324, sept. 2019.
[27] J. A. Purton, G. D. Barrera, N. L. Allan, et J. D. Blundy, « Monte Carlo and Hybrid Monte Carlo/Molecular Dynamics Approaches to Order- Disorder in Alloys, Oxides, and Silicates », *J. Phys. Chem. B*, vol. 102, n° 26, p. 5202–5207, 1998.
[28] P. Ungerer, B. Tavitian, and A. Boutin, « Applications of Molecular Simulation in the Oil and Gas Industry: Monte Carlo Methods (Ed. Technip, 2005) ».
[29] GIBBS, « http://pagesperso.lcp.u-psud.fr/rousseau/gibbs.html ».
[30] M. S. Daw et M. I. Baskes, « Embedded-atom method: Derivation and application to impurities, surfaces, and other defects in metals », *Phys. Rev. B*, vol. 29, n° 12, p. 6443‑6453, juin 1984.
[31] M. W. D. Cooper, S. T. Murphy, M. J. D. Rushton, et R. W. Grimes, « Thermophysical properties and oxygen transport in the (Ux,Pu1−x)O2 lattice », *J. Nucl. Mater.*, vol. 461, p. 206‑214, juin 2015.

[32] A. Zunger, S.-H. Wei, L. G. Ferreira, et J. E. Bernard, « Special quasirandom structures », *Phys. Rev. Lett.*, vol. 65, n° 3, p. 353‑356, juill. 1990.
[33] P. Soven, « Coherent-Potential Model of Substitutional Disordered Alloys », *Phys. Rev.*, vol. 156, n° 3, p. 809‑813, avr. 1967.
[34] L. Nordheim, « Zur Elektronentheorie der Metalle. II », *Ann. Phys.*, vol. 401, n° 6, p. 641‑678, 1931.
[35] M. Jaros, « Electronic properties of semiconductor alloy systems », *Rep. Prog. Phys.*, vol. 48, n° 8, p. 1091‑1154, août 1985.
[36] S.-H. Wei, L. G. Ferreira, J. E. Bernard, et A. Zunger, « Electronic properties of random alloys: Special quasirandom structures », *Phys. Rev. B*, vol. 42, n° 15, p. 9622‑9649, nov. 1990.
[37] J. von Pezold, A. Dick, M. Friák, et J. Neugebauer, « Generation and performance of special quasirandom structures for studying the elastic properties of random alloys: Application to Al-Ti », *Phys. Rev. B*, vol. 81, n° 9, mars 2010.
[38] T. Truphémus *et al.*, « Structural studies of the phase separation in the UO2–PuO2–Pu2O3 ternary system », *J. Nucl. Mater.*, vol. 432, n° 1‑3, p. 378‑387, janv. 2013.
[39] D. G. Martin, « The thermal expansion of solid UO2 and (U, Pu) mixed oxides—a review and recommendations », *J. Nucl. Mater.*, vol. 152, n° 2‑3, p. 94–101, 1988.
[40] Fritz I, « J. Appl. Phys. 47 4353 ».
[41] R. Kandan, R. Babu, K. Nagarajan, et P. R. Vasudeva Rao, « Calorimetric measurements on uranium–plutonium mixed oxides », *J. Nucl. Mater.*, vol. 324, n° 2‑3, p. 215‑219, janv. 2004.
[42] I. C. Njifon, M. Bertolus, R. Hayn, et M. Freyss, « Electronic Structure Investigation of the Bulk Properties of Uranium–Plutonium Mixed Oxides (U, Pu)O_2 », *Inorg. Chem.*, vol. 57, n° 17, p. 10974‑10983, sept. 2018.
[43] Cheik Njifon Ibrahim, *Modélisation des modifications structurales, électroniques et thermodynamiques induites par les défauts ponctuels dans les oxydes mixtes (U,Pu)O2*. Thèse AMU, 2018.
[44] R. Vauchy, A.-C. Robisson, F. Audubert, et F. Hodaj, « Ceramic processing of uranium–plutonium mixed oxide fuels (U1−yPuy)O2 with high plutonium content », *Ceram. Int.*, vol. 40, n° 7, p. 10991‑10999, août 2014.
[45] T. Yamashita, N. Nitani, T. Tsuji, et H. Inagaki, « Thermal expansions of NpO2 and some other actinide dioxides », *J. Nucl. Mater.*, vol. 245, n° 1, p. 72–78, 1997.
[46] W. L. LYON, « THE SOLID-LIQUID PHASE DIAGRAM FOR THE UOz-PuOz SYSTEM + », p. 8.
[47] J. K. Fink, « Thermophysical properties of uranium dioxide », *J. Nucl. Mater.*, p. 18, 2000.
[48] L. Vegard, « Die konstitution der mischkristalle und die raumfüllung der atome », *Z. Für Phys.*, vol. 5, n° 1, p. 17–26, 1921.
[49] A. Grossfield et D. M. Zuckerman, « Chapter 2 Quantifying Uncertainty and Sampling Quality in Biomolecular Simulations », in *Annual Reports in Computational Chemistry*, vol. 5, Elsevier, 2009, p. 23‑48.
[50] M. Lagache, P. Ungerer, A. Boutin, et A. H. Fuchs, « Prediction of thermodynamic derivative properties of fluids by Monte Carlo simulation », *Phys. Chem. Chem. Phys.*, vol. 3, n° 19, p. 4333‑4339, 2001.
[51] T. Uchida, T. Sunaoshi, K. Konashi, et M. Kato, « Thermal expansion of PuO2 », *J. Nucl. Mater.*, vol. 452, n° 1‑3, p. 281‑284, sept. 2014.
[52] « J.A. Fahey, R.P. Turcotte and T.D. Chikalla, Inorg. Nucl. Chem. Lett. 10 (1974) 459 ».
[53] M. Tokar, A. W. Nutt, et T. K. Keenan, « Linear Thermal Expansion of Plutonium Dioxide », *Nucl. Technol.*, vol. 17, n° 2, p. 147‑152, févr. 1973.
[54] J.M. Leblanc and H. Andriessen, « EURATOM/USA Rep. EURAEC-434 (1962) ».
[55] N.H. Brett and L.E. Russel, « Plutonium 1960 (Cleaver Hume Press Ltd., London, 1961) p. 397 ».
[56] P. Martin *et al.*, « XAS study of (U1−yPuy)O2 solid solutions », *J. Alloys Compd.*, vol. 444‑445, p. 410‑414, oct. 2007.

[57] M. W. D. Cooper, « Thermophysical properties and oxygen transport in the (Ux,Pu1−x)O2 lattice - ScienceDirect ». [En ligne]. Disponible sur: http://www.sciencedirect.com/science/article/pii/S0022311515001701#bb0140. [Consulté le: 19-janv-2018].
[58] R. Merkle et J. Maier, « On the Tammann-Rule », *Z. For Anorg. Allg. Chem.*, vol. 631, n° 6‑7, p. 1163‑1166, mai 2005.
[59] Golunski SE, . « Why use platinum in catalytic converters? Platin Met Rev 51, 162-162 (2007) ».
[60] A. Annamareddy et J. Eapen, « Low Dimensional String-like Relaxation Underpins Superionic Conduction in Fluorites and Related Structures », *Sci. Rep.*, vol. 7, n° 1, déc. 2017.
[61] A. Annamareddy et J. Eapen, « Disordering and dynamic self-organization in stoichiometric UO2 at high temperatures », *J. Nucl. Mater.*, vol. 483, p. 132‑141, janv. 2017.
[62] V. A. Annamareddy, P. K. Nandi, X. Mei, et J. Eapen, « Waxing and waning of dynamical heterogeneity in the superionic state », p. 9.
[63] K. Clausen, W. Hayes, J. E. Macdonald, R. Osborn, et M. T. Hutchings, « Observation of Oxygen Frenkel Disorder in Uranium Dioxide above 2000 K by Use of Neutron-Scattering Techniques », *Phys. Rev. Lett.*, vol. 52, n° 14, p. 1238‑1241, avr. 1984.
[64] M. J. Gillan, « Collective dynamics in superionic CaF_2 . I. Simulation compared with neutron-scattering experiment », *J. Phys. C Solid State Phys.*, vol. 19, n° 18, p. 3391‑3411, juin 1986.
[65] M. J. Gillan, « Collective dynamics in super-ionic CaF_2 . II. Defect interpretation », *J. Phys. C Solid State Phys.*, vol. 19, n° 19, p. 3517‑3533, juill. 1986.
[66] M. J. Gillan, « Collective dynamics in superionic CaF_2 . I. Simulation compared with neutron-scattering experiment », *J. Phys. C Solid State Phys.*, vol. 19, n° 18, p. 3391‑3411, juin 1986.
[67] J. P. Hiernaut, G. J. Hyland, et C. RonchP, « Premelting transition in uranium dioxide », p. 25.
[68] Hyland, G.J.; Ralph, J., « Electronic contributions to the high-temperature thermophysical properties of UOsub(2+x): a critical analysis », *High Temp. - High Press. ISSN 0018-1544 V 152 P 179-190*, 1983.
[69] T. R. Pavlov *et al.*, « Measurement and interpretation of the thermo-physical properties of UO 2 at high temperatures: The viral effect of oxygen defects », *Acta Mater.*, vol. 139, p. 138‑154, oct. 2017.
[70] M. W. D. Cooper, S. C. Middleburgh, et R. W. Grimes, « Modelling the thermal conductivity of (UxTh1−x)O2 and (UxPu1−x)O2 », *J. Nucl. Mater.*, vol. 466, p. 29‑35, nov. 2015.
[71] H. Zhang, X. Wang, A. Chremos, et J. F. Douglas, « Superionic UO2: A Model Anharmonic Crystalline Material », p. 57.
[72] L.-M. Wang, C. A. Angell, et R. Richert, « Fragility and thermodynamics in nonpolymeric glass-forming liquids », *J. Chem. Phys.*, vol. 125, n° 7, p. 074505, août 2006.
[73] R. G. Beaman, « Relation between (apparent) second-order transition temperature and melting point », *J. Polym. Sci.*, vol. 9, n° 5, p. 470‑472, nov. 1952.
[74] R. D. Shannon et C. T. Prewitt, « Effective ionic radii in oxides and fluorides », *Acta Crystallogr. B*, vol. 25, n° 5, p. 925‑946, mai 1969.
[75] J. K. Fink, « Enthalpy and Heat Capacity of the Actinide Oxides », *Int. J. Thermophys. Vol 3 No 2 1982*.
[76] R. J. M. Konings *et al.*, « The Thermodynamic Properties of the *f* -Elements and their Compounds. Part 2. The Lanthanide and Actinide Oxides », *J. Phys. Chem. Ref. Data*, vol. 43, n° 1, p. 013101, mars 2014.
[77] W. L. Jorgensen, « Optimized intermolecular potential functions for liquid alcohols », *J. Phys. Chem.*, vol. 90, n° 7, p. 1276‑1284, mars 1986.
[78] Hiroyuki Serizawa et al., « Simultaneous determination of X-ray Debye temperature and Gruneisen constant for actinide dioxides: PuO2 and ThO2 », *J. Nucl. Mater. 280 2000 99±105*.
[79] J. P. Hiernaut, G. J. Hyland, et C. RonchP, « Premelting transition in uranium dioxide », p. 25.
[80] C. Guéneau *et al.*, « Thermodynamic modelling of advanced oxide and carbide nuclear fuels: Description of the U–Pu–O–C systems », *J. Nucl. Mater.*, vol. 419, n° 1‑3, p. 145‑167, déc. 2011.

[81] M. G. Adamson, E. A. Aitken, et R. W. Caputi, « Experimental and thermodynamic evaluation of the melting behavior of irradiated oxide fuels », *J. Nucl. Mater.*, vol. 130, p. 349‑365, févr. 1985.
[82] R. Böhler *et al.*, « Recent advances in the study of the UO2–PuO2 phase diagram at high temperatures », *J. Nucl. Mater.*, vol. 448, n° 1‑3, p. 330‑339, mai 2014.
[83] M. Jeffroy, « Simulation moléculaire des propriétés des zéolithes cationiques: Propriétés thermodynamiques et propriétés structurales », PhD Thesis, Université Paris Sud-Paris XI, 2010.
[84] E. Yakub, C. Ronchi, et D. Staicu, « Molecular dynamics simulation of premelting and melting phase transitions in stoichiometric uranium dioxide », *J. Chem. Phys.*, vol. 127, n° 9, p. 094508, sept. 2007.
[85] A. V. Lunev et B. A. Tarasov, « A classical molecular dynamics study of the correlation between the Bredig transition and thermal conductivity of stoichiometric uranium dioxide », *J. Nucl. Mater.*, vol. 415, n° 2, p. 217‑221, août 2011.
[86] M. A. Korneva et S. V. Starikov, « Atomistic simulation of a superionic transition in UO2 », *Phys. Solid State*, vol. 58, n° 1, p. 177‑182, janv. 2016.
[87] M. Yu. Lavrentiev, N. L. Allan, et C. Wragg, « Lithium oxide: a quantum-corrected and classical Monte Carlo study », *Phys. Chem. Chem. Phys.*, vol. 21, n° 27, p. 14964‑14972, 2019.
[88] M. Kato, T. Uchida, T. Matsumoto, T. Sunaoshi, H. Nakamura, et M. Machida, « Thermal expansion measurement and heat capacity evaluation of hypo-stoichiometric PuO2.00 », *J. Nucl. Mater.*, vol. 451, n° 1‑3, p. 78‑81, août 2014.
[89] H. Nakamura, M. Machida, et M. Kato, « LDA+ U study on plutonium dioxide with spin-orbit couplings », *Prog. Nucl. Sci. Technol.*, vol. 2, p. 16–19, 2011.
[90] H. Nakamura, M. Machida, et M. Kato, « Effects of spin-orbit coupling and strong correlation on the paramagnetic insulating state in plutonium dioxides », *Phys. Rev. B*, vol. 82, n° 15, oct. 2010.
[91] T. Hotta, H. Harima, « T. Hotta, H. Harima, J. Phys. Soc. Jpn. 75 (2006) 124711 ».
[92] F. L. Oetting, « The chemical thermodynamics of nuclear materials. VII. the high-temperature enthalpy of plutonium dioxide », *J. Nucl. Mater.*, vol. 105, n° 2‑3, p. 257–261, 1982.
[93] S. I. Potashnikov, A. S. Boyarchenkov, K. A. Nekrasov, et A. Y. Kupryazhkin, « High-precision molecular dynamics simulation of UO2–PuO2: superionic transition in uranium dioxide », p. 7.
[94] M. Idiri, T. Le Bihan, S. Heathman, et J. Rebizant, « Behavior of actinide dioxides under pressure: U O 2 and Th O 2 », *Phys. Rev. B*, vol. 70, n° 1, juill. 2004.
[95] P.Browning, « THERMODYNAMIC PROPERTIES OF URANIUM DIOXIDE: A STUDY OF THE EXPERIMENTAL ENTHALPY AND SPECIFIC HEAT », *J. Nucl. Mater.*, vol. 98, p. 345‑356, 1981.
[96] « ESNII+ Deliverable_D7-51_Catalog.pdf ». .
[97] T. Arima, S. Yamasaki, Y. Inagaki, et K. Idemitsu, « Evaluation of thermal properties of UO2 and PuO2 by equilibrium molecular dynamics simulations from 300 to 2000K », *J. Alloys Compd.*, vol. 400, n° 1‑2, p. 43‑50, sept. 2005.
[98] C. H. de Novion, B. Amice, A. Groff, Y. Guerin and A. Pade, « Mechanical Properties of Uranium Plutonium Based Ceramics, Nucl. Metall. 17 (1970) 509 ».
[99] A. W. Nutt, A. W. Allen, et J. H. Handwerk, « Elastic and Anelastic Response of Polycrystalline UO2-PuO2 », *J. Am. Ceram. Soc.*, vol. 53, n° 4, p. 205–210, 1970.